Unclassified/ unlimited

SECURITY CLASSIFICATION OF THIS PAGE (When Data Entered)

REPORT DOCUMENTATION PAGE

READ INSTRUCTIONS BEFORE COMPLETING FORM

1. REPORT NUMBER: N00014-85-C-0141-AR5
2. GOVT ACCESSION NO.: A161333
3. RECIPIENT'S CATALOG NUMBER:

4. TITLE (and Subtitle): RESEARCH ON ACOUSTICAL SCATTERING, OPTICS OF BUBBLES, DIFFRACTION CATASTROPHES, AND LASER GENERATION OF SOUND BY BUBBLES

5. TYPE OF REPORT & PERIOD COVERED: Annual Summary Report
1 Oct. 84 - 30 Sept. 85

6. PERFORMING ORG. REPORT NUMBER:

7. AUTHOR(s): Philip L. Marston

8. CONTRACT OR GRANT NUMBER(s): N00014-85-C-0141 and N00014-80-C-0838

9. PERFORMING ORGANIZATION NAME AND ADDRESS:
Department of Physics
Washington State University
Pullman, WA 99164-2814

10. PROGRAM ELEMENT, PROJECT, TASK AREA & WORK UNIT NUMBERS:
Program Element: 61153N
Task Area: RR011-08-01
Work Unit: NR384-934

11. CONTROLLING OFFICE NAME AND ADDRESS:
Physics Division Office (Code 412)
Office of Naval Research
Arlington, VA 22217

12. REPORT DATE: September 1985

13. NUMBER OF PAGES: 67 + v

14. MONITORING AGENCY NAME & ADDRESS(if different from Controlling Office):

15. SECURITY CLASS. (of this report): Unclassified/unlimited

15a. DECLASSIFICATION/DOWNGRADING SCHEDULE:

16. DISTRIBUTION STATEMENT (of this Report)

Approved for public release; distribution unlimited

17. DISTRIBUTION STATEMENT (of the abstract entered in Block 20, if different from Report)

18. SUPPLEMENTARY NOTES

Research done in cooperation with the following current or former graduate students: W. P. Arnott, K. L. Williams, and B. T. Unger. Telephone number for P. L. Marston: (509) 335-5343 or 335-9531.

19. KEY WORDS (Continue on reverse side if necessary and identify by block number)

Acoustic scattering, Inverse scattering, Resonance scattering theory, Back-scattering, Sonar calibration, Physical acoustics, Underwater acoustics, Light scattering, Bubbles, Mie theory, Optical oceanography, Light extinction, Optoacoustics, Photoacoustics, Rayleigh waves, Catastrophe Optics, Diffraction Catastrophes.

20. ABSTRACT (Continue on reverse side if necessary and identify by block number)

The research summarized concerns several aspects of the propagation and scattering of acoustical and optical waves. The topics discussed fall under the following four categories:

DD FORM 1 JAN 73 1473 EDITION OF 1 NOV 65 IS OBSOLETE
S/N 0102-LF-014-6601

Unclassified/ unlimited
SECURITY CLASSIFICATION OF THIS PAGE (When Data Entered)

20. Abstract (continued)

A. Acoustical scattering theory and experiments (focused backscattering from elastic spheres due to Rayleigh waves and resonances, Sommerfeld-Watson transformation or predicting echo amplitudes and resonance phenomena, scattering from complicated elastic objects);

B. Novel manifestations of diffraction catastrophes and their application to inverse problems (optical hyperbolic-umbilic and cusp diffraction catastrophes in the scattering from a penetrable spheroid, angular location of the cusp as a method of inverse scattering, calculation of the shape of the wavefront which produces a directional cusp diffraction catastrophe);

C. Production of sound by a bubble in water illuminated by modulated light (bubbles as a novel photoacoustic source, photoacoustics as a method of investigating adsorbed films or bubbles in water);

D. Light scattering from real bubbles in water (optical backscattering from freely rising bubbles in water, the unfolded glory of an oblate bubble, optical effects of adsorbed films).

DEPARTMENT OF PHYSICS

WASHINGTON STATE UNIVERSITY

PULLMAN, WA 99164-2814

REPORT NUMBER N00014-85-C-0141-AR5

ANNUAL SUMMARY REPORT NO. 5

SEPTEMBER, 1985

RESEARCH ON ACOUSTICAL SCATTERING, OPTICS OF BUBBLES, DIFFRACTION CATASTROPHES, AND LASER GENERATION OF SOUND BY BUBBLES

by

Philip L. Marston

Prepared for:

OFFICE OF NAVAL RESEARCH

CONTRACT NO. N00014-85-C-0141

TABLE OF CONTENTS

I. External Communications Supported by this Contract (since October 1, 1984):

A. Publications

1. K. L. Williams and P. L. Marston, "Mixed-Mode Acoustical Glory Scattering from a Large Elastic Sphere: Model and Experimental Verification," Journal of the Acoustical Society of America 76, 1555-1563 (1984).

2. P. L. Marston and J. H. Crichton, "Radiation Torque on a Sphere Caused by a Circularly Polarized Electromagnetic Wave," Physical Review A 30, 2508-2516 (1984).

3. P. L. Marston and E. H. Trinh, "Hyperbolic umbilic diffraction catastrophe and rainbow scattering from spheroidal drops," Nature (London) 312, 529-531 (1984).

4. P. L. Marston and S. G. Goosby, "Ultrasonically stimulated low-frequency oscillation and breakup of immiscible liquid drops: Photographs," Physics of Fluids 28, 1233-1242 (1985).

5. K. L. Williams and P. L. Marston, "Axially Focused (Glory) Scattering due to Surface Waves Generated on Spheres: Model and Experimental Confirmation using Tungsten Carbide Spheres," Journal of the Acoustical Society of America 78, 722-728 (1985).

6. K. L. Williams and P. L. Marston, "Backscattering from an elastic sphere: Sommerfeld-Watson transformation and experimental confirmation," Journal of the Acoustical Society of America 78, 1093-1102 (1985).

7. K. L. Williams and P. L. Marston, "Resonance Scattering Theory revisited via the Sommerfeld-Watson Transformation for scattering from elastic spheres," Journal of the Acoustical Society of America (submitted for publication).

8. P. L. Marston and B. T. Unger, "Rapid Cavitation Induced by the Reflection of Shock Waves" (submitted to Shock Waves in Condensed Matter, Y. M. Gupta, editor, Plenum Press).
9. P. L. Marston, "Cusp diffraction catastrophe from spheroids: generalized rainbows and inverse scattering," Optics Letters (accepted for publication).
10. P. L. Marston and D. S. Langley, "Forward optical glory from bubbles (and clouds of bubbles) in liquids and other novel directional caustics," Journal of Wave-Material Interaction (submitted to a special conference proceedings issue to be edited by V. K. and V. V. Varadan).
11. P. L. Marston and J. H. Crichton, "Radiation torque on a sphere illuminated with circularly polarized light and the angular momentum of scattered radiation," in Proceedings of the Chemical Research and Development Center's 1984 Scientific Conference on Obscuration and Aerosol Research, edited by R. H. Kohl and D. Stroud (U.S. Army, Aberdeen Proving Ground, MD, 1985) pp. 233-238.
12. P. L. Marston and D. S. Langley, "Transmitted wave and rainbow-enhanced glories of dielectric spheres," in the same Proceedings as the preceding item, pp. 239-240.

B. Abstracts of papers (presented at meetings) containing significant information not yet published (or submitted for publication) in final form.

1. P. L. Marston and D. S. Langley, "Optical scattering properties of bubbles of interest in acoustics and cavitation research," J. Acoust. Soc. Am. 76, S30 (1984).

2. B. T. Unger and P. L. Marston, "Optically stimulated sound from gas bubbles in water: A novel optoacoustic mechanism," J. Acoust. Soc. Am. 77, S104 (1985).

C. Reports issued

1. P. L. Marston, Annual Summary Report No. 4: Research on Acoustical And Optical Scattering, Optics of Bubbles, Diffraction Catastrophes, Laser Generation of Sound, and Shock Induced Cavitation, Accession Number AD-A146703 (Defense Technical Information Center, Alexandria, VA, issued September, 1984).
2. D. S. Langley, Technical Report No. 4: Light Scattering from Bubbles in Liquids, Accession Number AD-A158736 (Defense Technical Information Center, Alexandria, VA, issued December 1984).
3. K. L. Williams, Technical Report No. 5: Acoustical Scattering from an Elastic Sphere in Water: Surface Wave Glory, Resonances, and the Sommerfeld-Watson Transformation for Amplitudes, Accession Number AD-A158884 (Defense Technical Information Center, Alexandria, VA, issued August 1985).

D. Ph.D. dissertation supported by this contract

1. K. L. Williams, "Acoustical Scattering from an Elastic Sphere in Water: Surface Wave Glory, Resonances, and the Sommerfeld-Watson Transformation for Amplitudes" (Physics Department, Washington State University, August, 1985).

II. Preface and Explanation of System Used for Citation of References

This report summarizes progress in research supported by the contract titled: "Propagation and Effects of Acoustical and Optical Waves." The emphasis of the report is on progress subsequent to that described in the

previous Annual Summary Report, item C1 in the preceding list of "External communications." However, for continuity, certain research items discussed there will also be mentioned. The principal sections (indicated by different Roman numerals) may be read independently of each other.

The following reference system is used in this report. References to recent external communications supported by this contract will be made by giving the section letter and number of the list given in Sec. I of the present report. For example, the first item listed in Sec. I is referenced as A1. Reference to other literature, including earlier work supported by this contract, are listed in Sec. VIII. The first item in that list is referenced as [1].

III. Acoustical Scattering Theory and Experiments

A. Motivation for this Research: An Overview

The general motivation for research into acoustic scattering is usually taken to be the identification of targets (or general elastic structures) from properties of echoes. It should be remembered, however, that scattering may also cause degradation of acoustic signals used for communications and other purposes and that scattering research gives insight into the radiation patterns from driven elastic structures. It may be thought that scattering from elastic spheres is too specialized of problem to be of any practical consequence; however, we intend to show that our understanding of the surface-wave contributions to directional caustics, which we have studied for spheres, is helpful for understanding the echoes from complicated elastic structures (see Sec. IIIG below). Furthermore, spheres are useful as calibration targets or as passive navigational beacons.

One important aspect of our research is our ability to model and measure scattering amplitudes not just in the exact backward direction but

also in near backward directions. It is shown in Sec. IIIB that the width of the diffraction lobes in near-backward directions are indicative of the target's size.

The research summarized here in Sec. IIIB-D was largely carried out by Kevin L. Williams as a Ph.D. dissertation project. This dissertation[C3,D1] was completed in July 1985 and Williams is to begin work on acoustical scattering problems at the Naval Coastal Systems Center (Panama City, FL) in September 1985. A new student, Steve Kargl, began working on acoustical scattering research in August 1985 with the partial support of this contract.

B. Angular Dependence of Focused Backscattering due to Rayleigh Waves on Elastic Spheres

When a short tone burst is incident on a tungsten carbide sphere in water, the backscattering response shows a decaying pulse train[1] which can be attributed to a specular reflection and repeated circumnavigations of other waves. We experimentally investigated the angular dependence of Rayleigh wave contributions as the receiver is moved away from the backscattering axis.[A5,C3,D1] Figure 1 shows a simplified diagram of the apparatus and Fig. 2 shows the specular reflection and decaying pulse train for an incident burst of four sine waves having $ka = 49.1$ where a is the sphere's radius and $k = 2\pi/\text{wavelength}$. Since a detailed description and analysis of this experiment has been published,[A5] only a brief overview will be presented here. Figure 3 shows the physical picture which results from our analysis of the scattering. Our analysis predicts that the aforementioned angular dependence can be approximately described by $J_0(\beta\gamma)$ where β depends on the frequency of the sinusoidal tone burst used (or equivalently the ka of the sphere) and γ measures the angle relative to the backscattering axis. We show how this form of angular dependence may be attributed to a weak axial focusing along

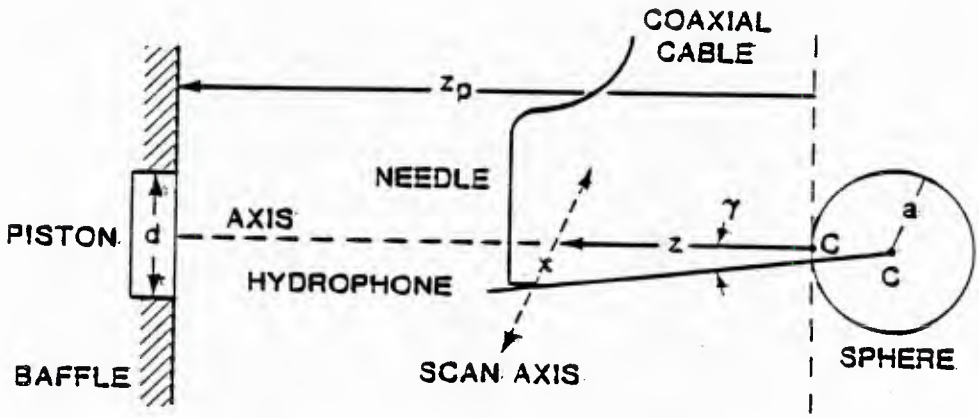

Simplified diagram of the scattering experiment. The backscattering angle is γ. The diagram is not drawn to scale. In all the experiments described in Section IIIB and C, $z_p \approx 160$ cm, while $z \approx 33$ cm for experiments with the 2.54 cm diameter tungsten carbide sphere and $z \approx 19$ cm for experiments with 1.27 cm sphere.

Fig. 1.

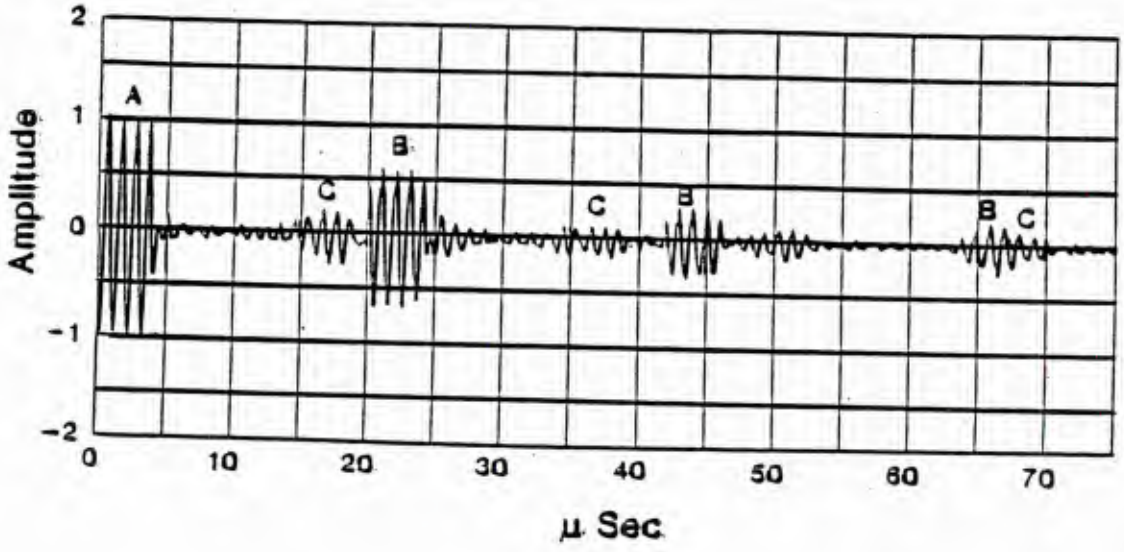

An oscilloscope trace of the backscattering echo from a tungsten carbide sphere ensonified by a tone burst. The ka of the sphere is approximately 49.1. The individual echoes are labeled as follows: A - specular reflection, B - Rayleigh surface wave echoes, C - echoes whose specific origin was not identified but which are conjectured to be other surface waves such as "Whispering Gallery" waves.

Fig. 2.

the backward direction. Our model includes a prediction of how β will vary with ka. The model is given in a general sense and then specialized to tungsten carbide for experimental confirmation.

Figure 4 shows that the measured angular dependence of the first Rayleigh echo amplitude is indeed of the form $J_0(\beta\gamma)$, shown by the curve. The parameter β was selected for agreement with the observations. This procedure was carried out for ka ranging from 30 to 100. The resulting experimental values of β were in good agreement with predictions, which for the size range studied is

$$\beta = (c/c_g)(ka - G) , \qquad (1)$$

where c is the sound speed in water, c_g is the group velocity of Rayleigh waves on the sphere (which must be nearly independent of ka for Eq. (1) to be useful) and G is a constant. The prediction of G required that the complex roots of a complex function be determined. See Eqs. (5) and (11) of Ref. A5. The computer programs used in this analysis are listed (or in some cases summarized) in Ref. C3 (which may be ordered from DTIC) and in Ref. D1.

Figure 4 also shows the normalized specular reflection amplitude (the squares) plotted as a function of γ. (These measurements were carried out late in 1984.) Only small fluctuations of the specular amplitude are evident since the specular echo is unfocused. This may be contrasted with the J_0 amplitude variation of the focused Rayleigh wave.

C. Backscattering from an Elastic Sphere: Sommerfeld-Watson Transformation and Experimental Confirmation

The prediction of the absolute amplitude of the Rayleigh echo was beyond the scope of the model described in Ref. A5. Such a prediction requires knowledge of the coupling efficiencies of sound to (and from)

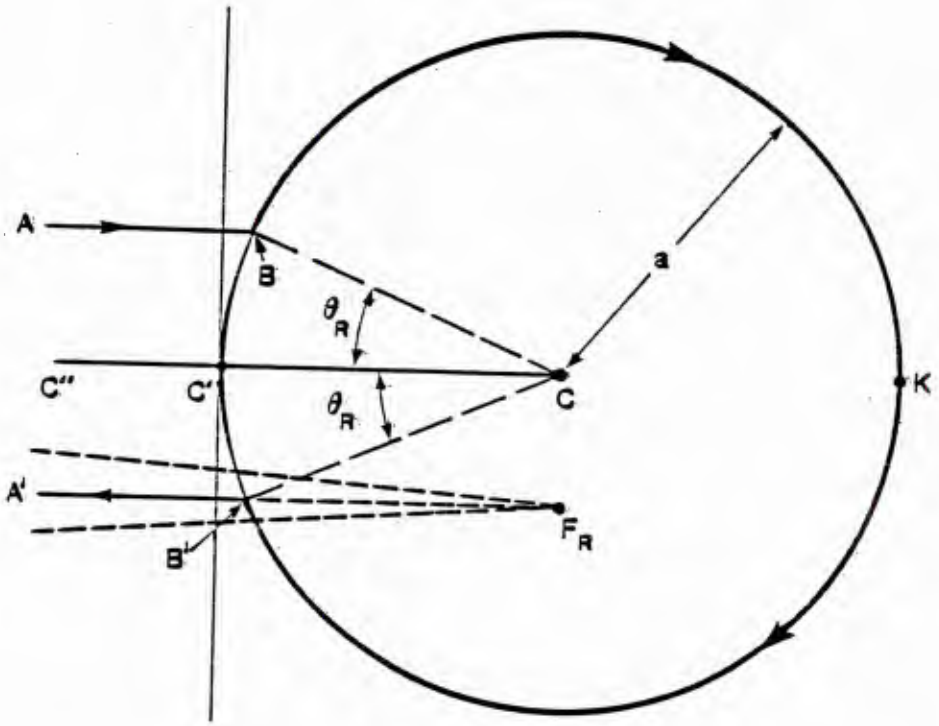

This figure shows the physical picture which ensues from the SWT analysis of the Rayleigh contributions to scattering. The incoming plane wave represented by AB allows the launching of a Rayleigh surface wave at B which circumnavigates the sphere while reradiating back into the surroundings. At point B′ energy is radiated in the backward direction F_R is the virtual point source from which ray A′B′ and the dashed rays to either side appear to originate. When the diagram is rotated around the C′C axis, the point F_R traces out a virtual ring-like source.

Fig. 3.

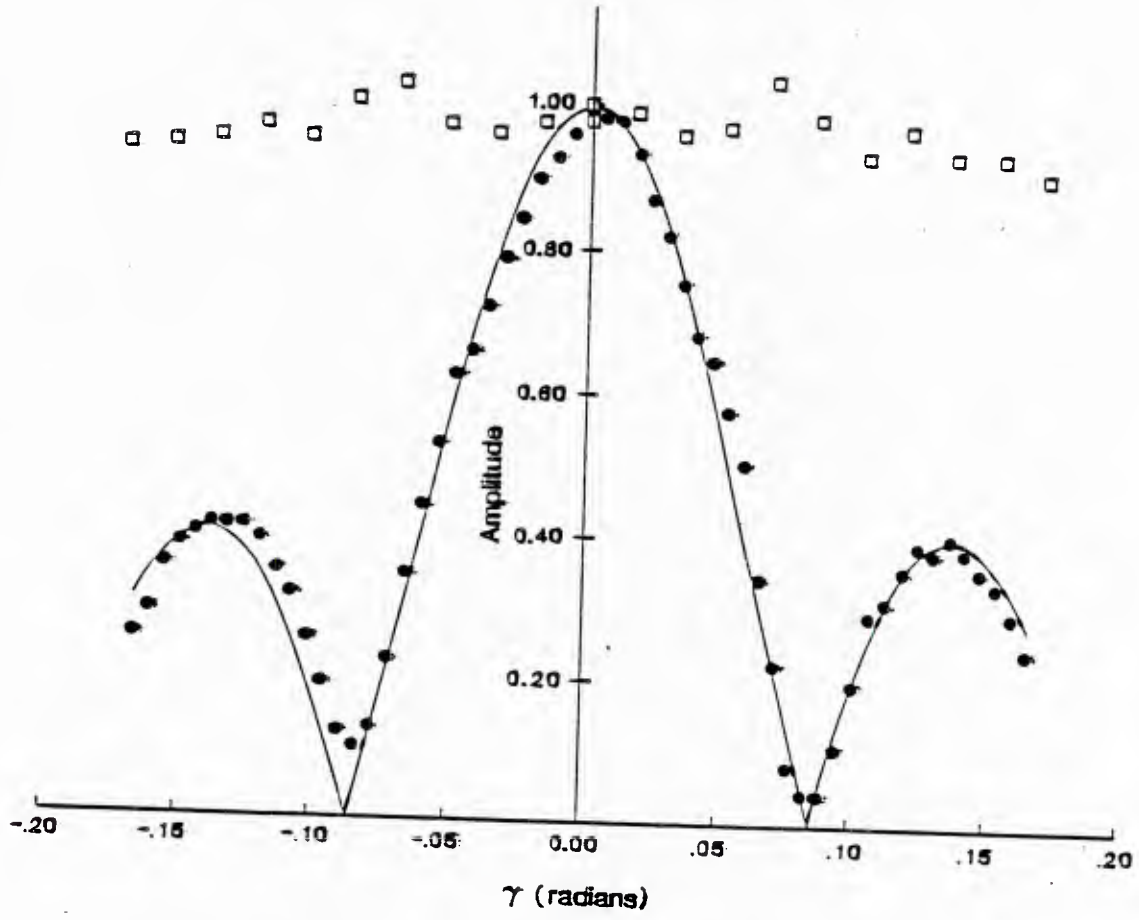

Experimental and theoretical results for ka = 60. The dots are experimental results of the angular dependence of the first Rayleigh echo amplitude normalized to the Rayleigh echo amplitude when γ, the backscattering angle, vanishes. The squares show experimental results for the specular reflection amplitude as a function of γ normalized to the specular reflection amplitude at $\gamma = 0$.

Fig. 4.

Rayleigh waves on a sphere as well as the radiation damping of Rayleigh waves. Our calculation of these quantities with a Sommerfeld-Watson Transformation (SWT) solves one of the canonical problems of acoustical scattering theory.[A6] Our analysis is not just applicable to Rayleigh waves on spheres, but it may be applied to a wide range of surface waves on spheres (such as to waves on spherical shells in water) provided the partial-wave series is available. Since our analysis is lengthy, and has been published in detail,[A6] only a brief overview of the results will be given here. Numerical evaluation of the echo amplitudes requires that the complex roots of a complex function be evaluated, see Eq. (23) of Ref. A6. The computer programs used for this evaluation are listed in Ref. C3 (which may be ordered from DTIC) and in Ref. D1.

The Rayleigh contribution to the form function for backward (and near backward) scattering is given by our analysis to be[A6]

$$f_R \simeq -G_R\, J_0(kb_R\gamma)\, e^{-\beta_R(2\pi-2\theta_R)}\, e^{i\eta_R} \sum_{m=0}^{\infty} e^{im(2\pi k_R a-\pi)}\, e^{-2\pi m\beta_R}, \qquad (2)$$

where the following parameters, which depend on ka and are given by expressions displayed in the publication (Ref. A6), have the following simple physical interpretations:

k_R = the wavenumber of the Rayleigh wave on the sphere = $(c/c_R)k$ where c_R is the Rayleigh phase velocity at the specified ka;

θ_R = $\arcsin(k/k_R)$ is the local angle of incidence where the sound in water is phase matched with the Rayleigh wave;

b_R = a $\sin\theta_R$ is the radius of the focal circle traced out when F_R in Fig. 5 is rotated around the CC′ axis;

η_R = a phase shift $\simeq -2ka\cos\theta_R + k_R a(2\pi - 2\theta_R) - \pi/2$;

β_R = the parameter which describes the attenuation of Rayleigh waves on the sphere which is given by Eq. (30) of Ref. A6 (the attenuation is due to radiation damping); do not confuse β_R with the β of Sec. IIIB;

G_R = the parameter which describes the coupling of sound on to (and off-of) the sphere and some of the effects of axial focusing. See Eq. (28) of Ref. A6.

The $m = 0$ term in Eq. (2) corresponds to the first (i.e. earliest) Rayleigh echo, the $m = 1$ term gives the second one, etc. Since Eq. (2) predicts the same J_0 dependence on γ as the model reviewed in Sec. IIIB, we limited our experimental effort to confirming that Eq. (2) gives the correct amplitudes for the $m = 0$ and $m = 1$ echoes when $\gamma = 0$.

To simplify the calibration of the experiment the procedure summarized below was used. The output voltage with the hydrophone (Fig. 1) positioned with $\gamma = 0$ gave time records like the one shown in Fig. 2. This was repeated for incident bursts having different values of ka. The following 3 peak-to-peak voltages were determined for each ka: V_S, which gives the specular amplitude and V_m ($m = 0$ and 1) giving the first two Rayleigh amplitudes. From these measurements, the ratios V_0/V_S and V_1/V_S were calculated. The upper group of points in Fig. 5 gives the V_0/V_S while the lower group gives V_1/V_S. The upper and lower curves follow from Eq. (2) with

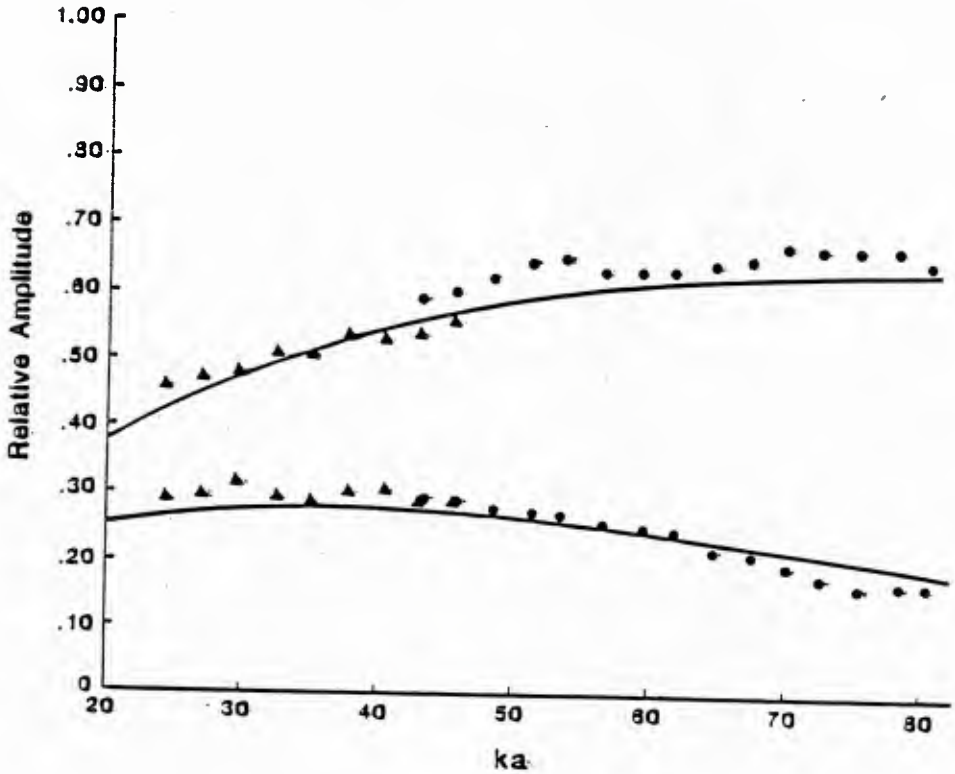

Experimental and theoretical results for the backscattering amplitudes of the first and second Rayleigh contributions as a function of ka. The amplitudes are normalized to the specular echo amplitude at the indicated value of ka. The dots are experimental results for the 2.54 cm diameter sphere, the triangles are results for the 1.27 cm diameter sphere, and the solid lines theoretical results using the SWT.

Fig. 5

$m = 0$ and 1 and from our SWT predictions of the specular amplitude.[A6] The agreement between experiment and theory is good enough to confirm our analysis. There is some uncertainty in the material parameters for these spheres and this may account for the small discrepancies evident.

It is noteworthy that the SWT facilitates a simple physical understanding of the ka dependence of the curves in Fig. 5. The interested reader should refer to the discussion section of Ref. A6.

D. Resonance Scattering Theory Revisited Via the Sommerfeld-Watson Transformation

One approach toward understanding the steady-state scattering from elastic objects, developed during the past decade,[2-4] is Resonance Scattering Theory (RST). The emphasis has largely been on the interpretation frequency dependence of the backscattered amplitude for elastic objects of simple shape. For example, Fig. 6 shows the exact form function f, computed by Williams,[C3,D1] for a tungsten carbide sphere in water; f is seen to fluctuate rapidly with ka. Also marked in Fig. 6 are the ka values of each (n,ℓ)th resonance where the circumference is equal to $n + (1/2)$ wavelengths of the ℓth surface wave type. The usual RST labeling prescription, discussed e.g. by Gaunaurd and Uberall,[4] was used. The $\ell = 1$ surface wave type corresponds to a Rayleigh wave on a tungsten carbide sphere while $\ell \geq 2$ corresponds to various whispering gallery waves.

One of the goals of the present research was to understand in detail the connection between the resonance locations and the fluctuations of f. What is unique about our procedure is that, for the first time, the direct results of the Sommerfeld Watson Transformation (SWT), summarized in Sec. IIIC, were used to quantitatively model f. It should be emphasized that the

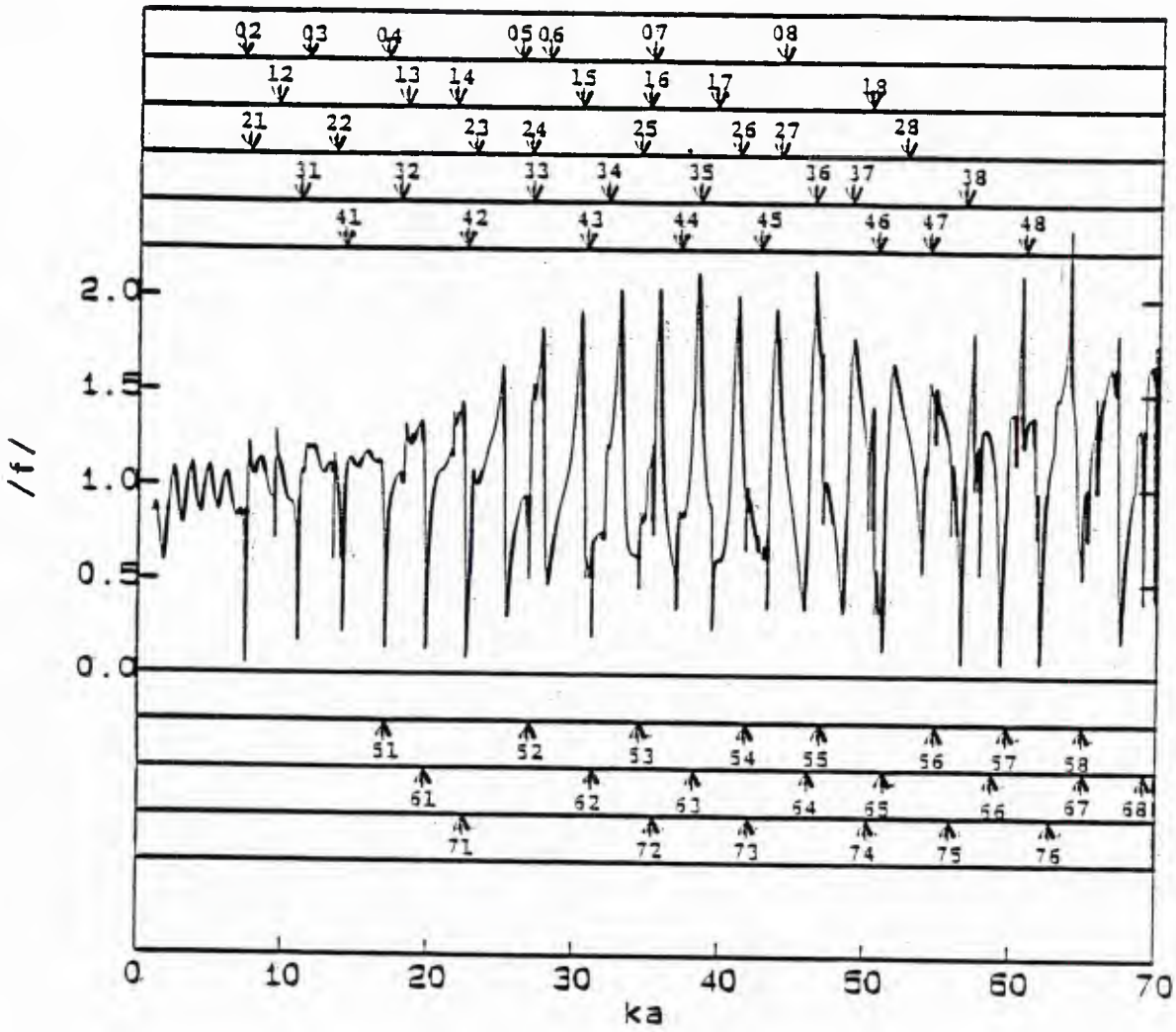

The backscattering form function of a tungsten carbide sphere as a function of ka. Also indicated by the arrows are the real part of the RST resonances for $n = 0-7$ and $\ell = 1-8$. The RST resonance locations were taken from Table IV of Ref. 4 and the figure is similar to Fig. 4 of the same reference.

Fig. 6.

procedure carried out is more generally applicable than to the specific target of tungsten carbide spheres considered (see Sec. IIIF).

The actual application of the SWT to the modeling of the form function and the critique of RST is not highly mathematical. For brevity, however, we will summarize only the principal results and the interested reader should consult Ref. A7, C3, or D1 for details. The computer programs used in this analysis are listed (or in some cases summarized) in Ref. C3 and D1. Our discussion will be limited to f in the exact backward direction ($\gamma = 0$ in Fig. 1). The method and results are summarized as follows:

(1) For each class ℓ of surface waves the geometric series in the corresponding SWT contribution to the form function may be summed analytically. The geometric series is shown for the case of a Rayleigh wave as the sum over m in Eq. (2), in Sec. IIIC of the resent report. The use of an analytic sum was motivated by the traditional analysis of optical Fabry-Perot resonators. The contribution to f (with $\gamma = 0$) for the ℓth class of waves becomes

$$f_\ell(ka) = \frac{-G_\ell \exp[-2(\pi-\theta_\ell)\beta_\ell + i\eta_\ell]}{\{1 + \exp[-2\pi\beta_\ell + i2\pi(\alpha_\ell + \tfrac{1}{2})]\}}, \qquad (3)$$

where the parameters are defined as in Eq. (2), for the specific case of a Rayleigh wave, but now for the more general surface wave. The new parameter is $\alpha_\ell = \mathrm{Re}\ \nu_\ell$ where ν_ℓ is the pole location in the complex ν plane, discussed in our original SWT paper, Ref. A6 but generalized here to the ℓth wave type.

(2) The correctness of this procedure was verified by computing the following approximate form function

$$f_{SR} = |f_S + f_R| , \tag{4}$$

where f_S is the specular contribution to f, given also by the SWT and f_R is the total Rayleigh wave contribution given by Eq. (3) with $\ell = 1$. Figure 7 compares f_{SR} with the exact modulus f_b of the form function given by the partial-wave series. It shows that f_{SR} reproduces much of the fluctuations in f except for a fine structure associated with whispering gallery waves (see below). The comparison was carried out for the entire region $10 \leq ka \leq 80$ and Fig. 7 is representative of the agreement observed.

Unlike the procedure of RST for which a local resonance contribution to f must be calculated for each (n,ℓ)th resonance, the present approximation gives the contribution to f for the ℓth wave type for all $ka >> 1$. This assertion was further confirmed by computing the following approximate form function

$$f_{SRWG} = |f_S + f_R + f_{WG1}| , \tag{5}$$

where f_{WG1}, given by Eq. (3) with $\ell = 2$, is the contribution to the form function of the slowest whispering gallery wave. Figure 8 compares f_{SRWG} with f_b. The comparison was carried out for the entire region $10 \leq ka \leq 80$ and Fig. 8 is representative of the agreement observed.

Inspection of Fig. 8 suggests that all resonance effects could be modeled with the aid of Eq. (3) by simply including additional surface waves, those having $\ell \geq 3$.

(3) The effect of a resonance on f_b is clearly not the same for each resonance. Our analysis[A7,C3,D1] shows that the phase difference between f_S and the f_ℓ greatly affects the shape of f_b near the (n,ℓ)th resonance. Thus at the resonance frequency predicted by RST, f_b need not have a minimum

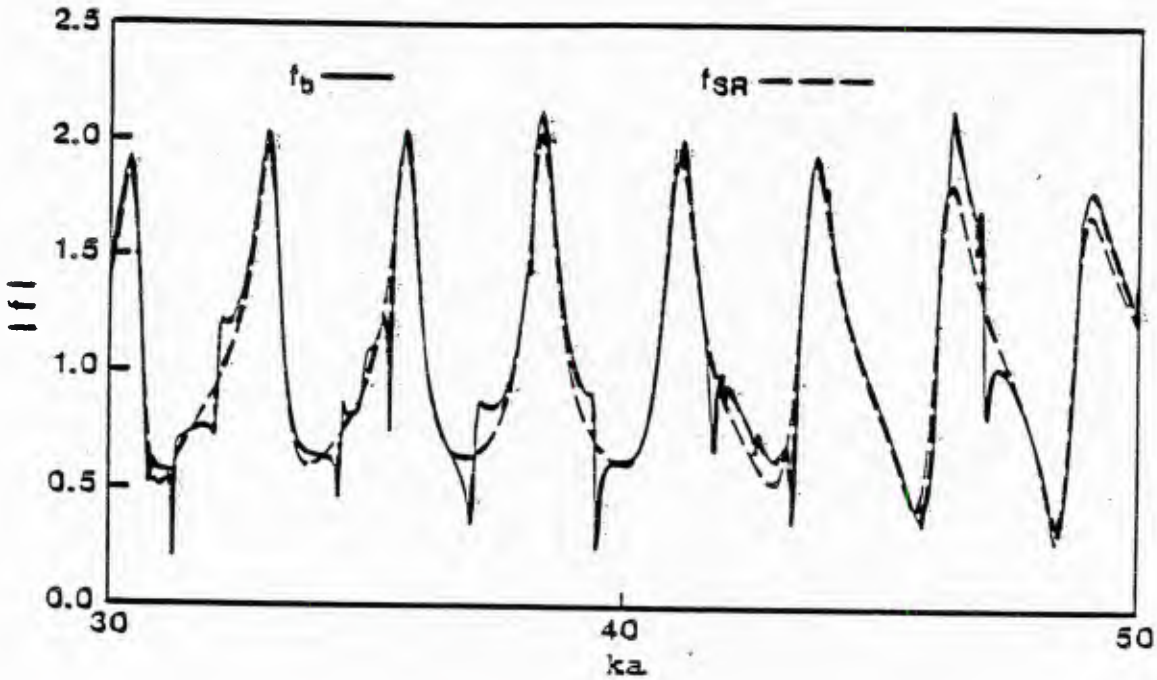
2.5
2.0
1.5
1.0
0.5
0.0
f_b
f_{SR}
30
40
50
ka

Fig. 7

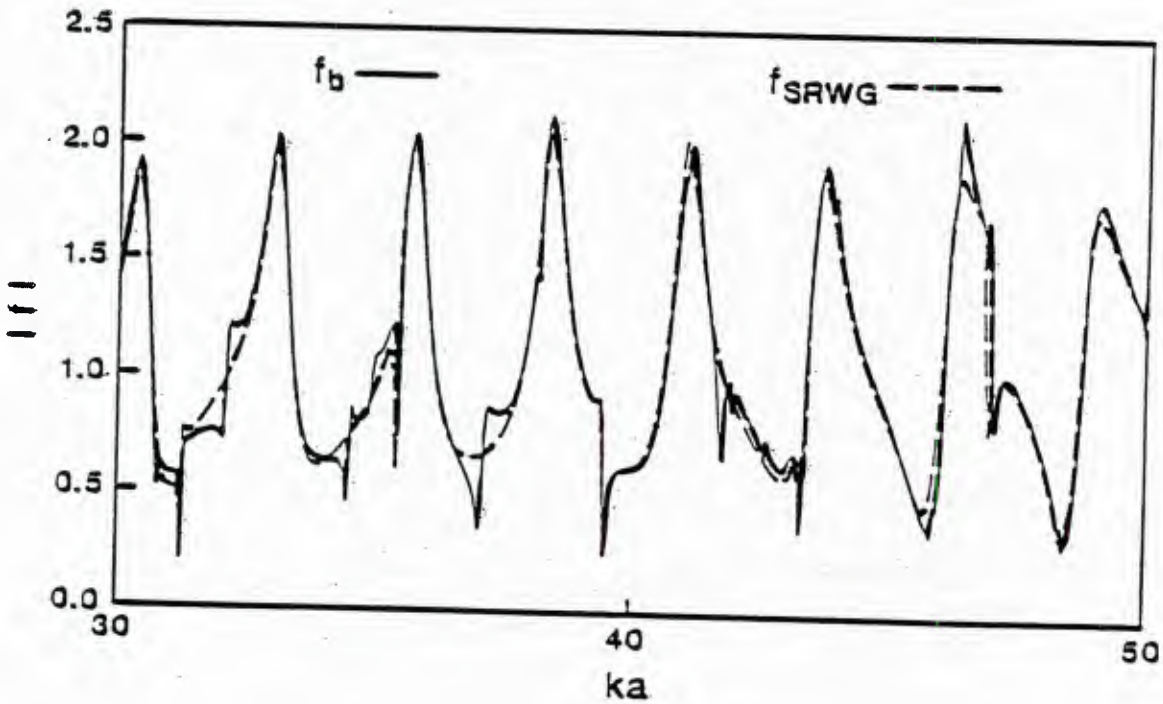
2.5
2.0
1.5
1.0
0.5
0.0
f_b
f_{SRWG}
30
40
50
ka

Fig. 8

(or for that matter a maximum). We have found this issue to be somewhat obscured in the literature on RST. The shape is also affected by the coupling parameter G_ℓ and the damping parameter β_ℓ.

(4) The resonance frequency for the (n,ℓ)th resonance of a sphere is defined to be that ka where by the circumference is equal to $n + (1/2)$ wavelengths of the ℓth surface wave. This condition on ka is equivalent to $\alpha_\ell = n$ in Eq. (3). For this ka, the magnitude of the denominator of Eq. (3) is close to minimum. The resulting ka value is found to differ from the actual resonance prescription used in RST. The apparent error in RST is usually small, it depends on value of β_ℓ. Furthermore, the prescription for the phase velocity of a surface wave given by RST is slightly in error when compared with the more exact presumption given by our SWT.

(5) Eq. (3) and our previous analysis of transmitted wave glories[A1] should facilitate an understanding of the ka dependence of f_b when ka is very large. Flax calculated f_b for aluminum spheres in water[6] for ka from 900 to 950; f_b was found to contain rapid fluctuations having different scales of quasi-periodicity. Resonances have been asserted to be the cause of these fluctuations;[4] however, we believe this interpretation to be incorrect for the following reasons: (i) We have computed the damping parameter β_ℓ for several surface waves on tungsten carbide, aluminum, and fused silica spheres. We find that β_ℓ increases with ka such that for very large ka the factor $\exp[-2(\pi - \theta_\ell)\beta_\ell]$ in Eq. (3) will be small because of excessive radiation damping. (ii) When ka is large, the number of distinct transmitted wave contributions[A1] to the form function becomes large. (In an SWT analysis, transmitted wave contributions are associated with saddle points of a contour integral while the resonances are associated with poles of an integrand.) It

is plausible that the interference of many distinct transmitted waves can cause rapid, pseudo-random, fluctuations of f_b. This has been discussed previously for the optical analog: the backscattering of light from spherical bubbles in liquids.[7]

E. SWT Calculations for Solid Spheres of Fused-Silica and Aluminum

As a guide to attempted (or planned) experiments with other target materials, Williams obtained numerically the fundamental parameters G_ℓ, β_ℓ, and $k_\ell a$ for range of ka for various Rayleigh and whispering gallery waves. These SWT computations were performed for solid spheres of fused-silica in water and aluminum in water.

F. Other Experiments on Scattering from Smooth and Rough Spheres in Water

Subsequent to the completion of the experiments discussed in Sec. IIIB and C, a new source transducer was obtained which permitted operation of the scattering facility at frequencies as low as 500 kHz. (A modification to facilitate a significant further reduction in frequency has recently been purchased.) Williams carried out preliminary scattering experiments with fused silica spheres in water having radii of 51.6 mm and 19.0 mm. These experiments manifest whispering gallery contributions to the backscattered echo train.

Williams also carried out some experiments on forward scattering by an artificially roughened sphere. Silicone grease was applied to the surface of a 37 mm radius sphere. A layer of sand (dia.~ 1 mm) was applied to the thin layer of grease to effect a roughening of the large sphere's surface. The specific goal of the experiment (Ref. 8 p. 13) was to demonstrate propagation

and focusing of the Biot-Tolstoy boundary wave mode[9] on a roughened sphere. The experiment was not successful; however, it was feasible to attempt the experiment with only a single frequency (~ 1 MHz) and scale of roughness at that time.

G. Applications of SWT and Models of Focused Scattering to Echo Prediction for Complicated Elastic Structures

The SWT and model results discussed in SEc. IIIB-D (see Fig. 3) should be applicable to modeling the elastic responses of some complicated structures. Recall that an air-filled spherical metal shell in water support propagating surface waves.[3] Instead of the Rayleigh and whispering gallery waves propagated in solid spheres (at moderate ka) one has waves analogous to those propagated on flat plates; e.g., Lamb waves. Such waves will produce axially focused backscattering having directional patterns similar in form to Fig. 4. To obtain the parameters G_ℓ, β_ℓ, and $k_\ell a$ so as to make use of Eq. (2) and (3) for spherical shells, it is first necessary to replace the B_n and D_n of Eqs. (A1) and (A2) of Ref. A6 by the determinants appropriate for a spherical shell.[10] The appropriate poles in the complex-ν plane must then be located.

It may be argued on physical grounds that various nonspherical structures can also produce axially-focused backscattering if appropriately insonified. A simple example is end-on insonification of a spheroid.[A5] Other examples include cylinders having hemispherical end-caps and isolated hemispheres. In the latter two cases, a range of directions should be possible for the incident wave such that surface-wave contributions to the scattering manifest focusing.

Our SWT analysis of axial focusing should be useful for understanding the radiation pattern from elastic shells at high frequencies. For example,

the excitation of a submerged spherical shell by an oscillating radial point-force gives rise to elastic surface waves ("structure-borne waves") on the shell.[11] The far-field radiation pattern will manifest axial focusing when a denominator in a coefficient corresponding to Eq. (3), is small. The largest focal effects would be seen along the axis (through the sphere's center) opposite the location of the excitation; however, focal effects should also be seen along the direction of the excitation if the relevant β_ℓ is small.

IV. Novel Manifestations of Diffraction Catastrophes and Their Application to Inverse Problems

A. Hyperbolic-Umbilic and Cusp Diffraction Catastrophes in the Scattering from a Penetrable Spheroid

In experiments partially supported by O.N.R. done with E. H. Trinh (Jet Propulsion Laboratory, Pasadena, California), Marston recently discovered that diffraction catastrophes, not previously known to appear, are present in the far-field scattering from spheroids.[A3,C1] This ranks as one of the most fundamental discoveries of rainbow phenomena subsequent to Airy's theory (1838) of diffraction at the rainbow caustic. Though the observations[A3] were of light scattered from spheroids, they are helpful for understanding some types of acoustical caustics. At the ordinary rainbow caustic considered by Airy, two rays merge to produce an unusually flat outgoing wavefront. At the caustic associated with the new "generalized rainbows," three or more rays merge[12] to produce a wavefront which is even flatter. (See Sec. VIC.) In the direction of far-field caustics, the Gaussian curvature K of the outgoing wavefront vanishes. Elementary geometrical optics predicts that the far-field amplitude is proportional to $K^{-1/2}$; hence the predicted amplitude has an unphysical divergence at caustics and diffraction gives an essential correction to the scattering amplitude.[13] The scattering amplitude near

caustics or "diffraction catastrophes" may be approximated using canonical diffraction integrals.[14] It is important to note however, that if the scatterer is significantly larger than the wavelength λ, parameters present in the diffraction integral may be determined geometrically. Thus it was proposed (Ref. 8 p. 14) to perform a skew-ray trace through a spheroid so as to calculate the axis ratio D/H of the oblate spheroids which produced the observed hyperbolic-umbilic foci where four rays merge. Prior to the completion of this calculation by Marston,[A9] it was done in late 1984 by Nye.[12] Marston and Nye obtain the same expression for the critical D/H; see Appendix I which is a reproduction of Ref. A9. The calculated D/H was in good agreement with the observations.[A3] See Fig. 3 of Appendix I for definitions of D and H.

Significant deviations of the axis ratio D/H from the critical value caused the observed diffraction patterns to separate into that of a cusp adjacent to a rainbow (Airy) pattern. See Fig. 2(a) and 2(c) of Appendix I; similar photographs were given in Ref. A3 and C1.

Prior to summarizing additional research on directional (far-field) diffraction catastrophes, it is appropriate to note the connection with propagation and scattering problems of interest in acoustics. The most obvious connection is that short-wavelength acoustical problems are analogous to ones in optics. It is much easier to observe optical diffraction patterns and consequently exploratory research on diffraction catastrophes is best carried out optically. Consider for example the diffraction of sound by a homogeneous penetrable spheroid at short wavelengths. If the sound speed of the interior is less than that of the surroundings, the acoustical scattering patterns will be similar to those shown in Fig. 2 of Appendix I for the analogous problem of light scattering from an oblate drop. Because of the

complexity of these patterns, however, it appears unlikely that they would have been recognized as diffraction catastrophes if only hydrophone data were available from an acoustic scattering experiment. It is, however, important to recognize diffraction catastrophes when they occur since then the wavefield throughout a region can be described with only a few parameters and known scaling laws[14] describe how changes in λ affect the amplitude and the pattern's width.

The real importance of Marston's study of far-field diffraction catastrophes is not so much that scattering from spheroids is important but instead that this study gives insight into a potentially broad range of phenomena. Diffraction catastrophe's occur whenever a few rays coalesce. Most optical studies of them have been concerned with near field catastrophes where the focal region is either close to the source or close to the scatterer.[14] Likewise, the acoustical cusp diffraction catastrophe was only previously studied for the longitudinal near-field focusing[15] near a "convergence zone." It is now clear from the optical experiments[A3,A9] that simple wavefronts can produce focusing transverse to the propagation direction such that the focal region extends out to infinity. It is clear that such directional caustics involving the coalescence of 3 or more rays will eventually be found for scattering and propagation of sound in the ocean or in other applications.

It is appropriate to note that the axial foci discussed in Sec. III (review Fig. 1-4) are a special directional caustic for which an infinite number of rays coalesce. The resulting focal pattern is usually described as "glory scattering" and not as a diffraction catastrophe since the wavefield is not "stable" with regard to small changes of the initial outgoing wavefront.

The distinction between glory scattering and diffraction catastrophes is further discussed in Ref. 8, 13, 14, and A10.

B. Angular Location of the Cusp and Inverse Scattering

For spheroids much larger than λ, the angular location of the cusp is determined by the axis ratio D/H. Consequently diffraction catastrophes may be useful for decoupling size and shape information in the scattering pattern. The size of the scatterer may be determined from the angular spacing of the structure in the pattern. Hence diffraction catastrophes should be useful for inverse scattering: the problem of identifying, the size, shape, and composition of a scatterer from its far-field scattering pattern. To illustrate the aforementioned decoupling, Marston calculated geometrically the angular location of the cusp.[A9] The calculation is summarized in Appendix I where Fig. 4 demonstrates experimental confirmation. This is a novel approach to the inversion of far-field optical scattering patterns of nonspherical objects; however, the ideas of catastrophe optics have been applied to the inversion of seismic reflection data[16] and other near-field inverse problems.

C. What Shape Must an Outgoing Wavefront be to Produce a Directional Cusp Diffraction Catastrophe?

Marston carried out a novel calculation of the wavefront's shape which gives rise to a cusp in the far field. (Recall that the right side of the Fig. 2(a) of Appendix I illustrates the cusp diffraction pattern.) It is well known that near-field cusps may be described in terms of the following one-dimensional diffraction integral commonly known as the Pearcey function[13-18]

$$P(X,Y) = \int_{-\infty}^{\infty} e^{i(s^4 + Xs^2 + Ys)} ds \ . \qquad (6)$$

This problem was solved by Marston by making use of several properties of $P(X,Y)$ including the result[17] that the geometric caustic lies on what is known as a "cuspidal cubic curve"

$$X^3 = -\frac{27}{8} Y^2 . \tag{8}$$

This curve is shown as the faint dashed line in Fig. 8; on the left of it, $d(s^4 + Xs^2 + Ys)/ds = 0$ has 3 distinct roots ($s = s_j$, $j = 1$-3) while on the right there is only one root. These roots must correspond to rays in the x,y plane of the outgoing wavefront. The result of the analysis is that f is of the form

$$f(x,y) = e^{i(b_1 x^2 + b_2 y^2 x)} , \tag{9}$$

where b_1 and b_2 are real constants. Then integration over x in Eq. (7b) results in $F \propto P$ with the aforementioned liner proportionalities satisfied. The stationary phase points of F map into those of P and Eq. (8) maps into a cuspoidal cubic curve having $\bar{\theta}^3 \propto \zeta^2$ with $\bar{\theta} \geq 0$. The Gaussian curvature K vanishes for points on the outgoing wave directed toward $\bar{\theta}$ and ζ on this cuspoidal curve.

The result, Eq. (9), is novel and not anticipated by previous studies (e.g. Ref. 13-18, 20) of cusp diffraction catastrophes. With $y = 0$ the phase reduces to $b_1 x^2$ which is the expected form. The term $b_2 y^2 x$ is crucial to the formation of a directional cusp; it is essential that $b_2 \neq 0$ if the directional cusp is to exist.

These results are consistent with the following results from abstract mathematics:

(a) The geometric singularity for the focusing of a one-dimensional wave whose diffraction integral reduces to Eq. (6) is classified

by Arnold[21] as an A_3 singularity. Arnold shows there is an invertable mapping (isomorphism) between classes of singularities and the Weyl groups. The specific singularity due to the focusing of a wave whose initial amplitude is $\exp(is^4)$, where s is a transverse coordinate, maps into the A_3 Weyl group.

(b) When a wave described by Eq. (9) comes to a focus, the resulting geometric singularity maps into the D_3 Weyl group. This may be seen by applying Arnold's form for the phase of a wave having a D_n singularity (usually only used for $n \geq 4$) to the specific case of $n = 3$.

(c) Finally, and most important, there is an equivalency relation between the A_3 and D_3 Weyl groups.[22]

It is also noteworthy that for the A_3 wave type, three rays merge at the most singular point of the energy flux while for the D_3 wave type three rays merge in the most singular direction.

Perhaps to certain mathematicians, Marston's derivation of Eq. (9) may have been unnecessary because of the aforementioned equivalency relation between Weyl groups; however, acousticians will find Marston's analysis to be the most direct approach. There are indications that additional optical studies of focused scattering will be helpful for understanding acoustic wave propagation.

V. Production of Sound by a Pre-existent Bubble in Water Illuminated by Modulated Light: A Novel Photo-Acoustic Source and Potential Tool for Investigating Adsorbed Films on Bubbles

A. Motivation for this Research and Review of Our Previous Work

It is well known that focused pulses of laser light having an energy of about 1J and duration 30 ns can breakdown water so as to create a vibrating bubble; such "laser-induced" cavitation radiates sound.[23] In the research supported by this contract, a completely new method for optical generation of sound related to bubbles has been demonstrated.[B2] Small bubbles which existed prior to illumination by a laser pulse having an energy ~10 μJ and duration ~5 μs were found to radiate sound. This novel photo-acoustic mechanism is being studied by a graduate student B. T. Unger, as a Ph.D. dissertation project.

Some of the mechanisms whereby optical energy may be converted by a pre-existent bubble to acoustical energy are[C1]: (i) the compression of the bubbles by optical radiation pressure and the resulting radiation of sound from the monopole oscillations of the bubble; and (ii) radiation associated with monopole oscillations driven by the heating and cooling of the gas within the bubble. (The heating being due to the absorption of light by the gas and by the bubble's surface "skin" or surroundings.) Mechanism (i) is particularly unusual in that unlike most photo-acoustic sources, the production of sound is not driven by thermal expansion and contraction.

The magnitude of the acoustic wave driven by (ii) will depend on the presence of molecules near the bubble which absorb the light. In principle such molecule could be present as a surface film on bubbles in water. If such films on bubbles could be characterized photoacoustically, it would be of

special interest in physical oceanography and acoustics. This is because adsorbed layers are thought by some researchers[24] to significantly affect acoustical damping and gas transport properties of bubbles in the ocean. Though we do not think we are studying such films in our present photo-acoustic experiments, the techniques which we have developed for detecting weak, optically-stimulated acoustic emissions from bubbles may be applicable to film characterization. Other optical methods for characterizing such films will be discussed in Sec. VIC.

During the previous contract period[C1] we had occasional success at using a CW laser to optically levitate a bubble by way of the radiation pressure of light. This provided a quiet environment whereby weak acoustic emission from a bubble, in response to the modulated output of a second laser, could be detected. Despite apparent detection of photoacoustic signals from bubbles by this technique[C1] we have gone over to a much simpler method of holding the bubble. This is because it was difficult to levitate on demand and also because of a decrease in the output power of one of the lasers. The signals detected in the new experiments (reported in the next section) are unambiguously caused by photoacoustic-emission from a bubble.

B. Detection of Photo-Acoustic Emission from Bubbles in Water

The progress reported here was for the period 1 October 1984 - 15 May 1985. During the period 15 May 1985 - 15 August 1985 Unger was on leave (and was not supported by the contract). Unger has returned to this research and is presently calibrating the apparatus.

We were requested by the American Institute of Physics to prepare a News Release descriptive of this research for broad distribution. This release is reproduced as Appendix II of this report. It should be of interest

to readers unfamiliar with general photo-acoustics and bubble dynamics. The research was also reported in Science News.[25]

Unger has used three methods of supporting single bubbles of gas. These are as follows:

(1) The bubble is in contact with a thin horizontal hypodermic needle. The air in the bubble does not communicate with the gas within the hollow needle once the bubble is formed.

(2) A bubble of H_2 gas is formed by electrolysis at a tungsten wire in water. The bubble floats upward from the wire and is trapped against a thin sheet (thickness ~ 6 μm) of transparent Mylar. The Mylar is supported by a wire loop having a diameter ~ 2 cm.

(3) The Mylar in method (2) is replaced by a thin glass plate (180 μm thick x 7 mm wide x 22 mm long).

The radii of the bubbles trapped by these methods were in the range 25 to 125 μm.

Figure 10(a) is a simplified diagram of the apparatus which shows the illumination path presently used. (Support method (3) is illustrated.) The bubble is illuminated by a pulse (or repeated pulses as discussed below) from the modulated output of an Ar-Ion laser having a maximum power output ≃ 2W. The laser is operated in the TEM01* mode which is usually described as the "doughnut" mode, because of an intensity minimum in the center of the beam. This pulsed beam is focused such that its outer diameter is somewhat larger than that of the bubble and its axis is centered on the bubble. As a consequence of the doughnut mode, most of the illumination impacts the

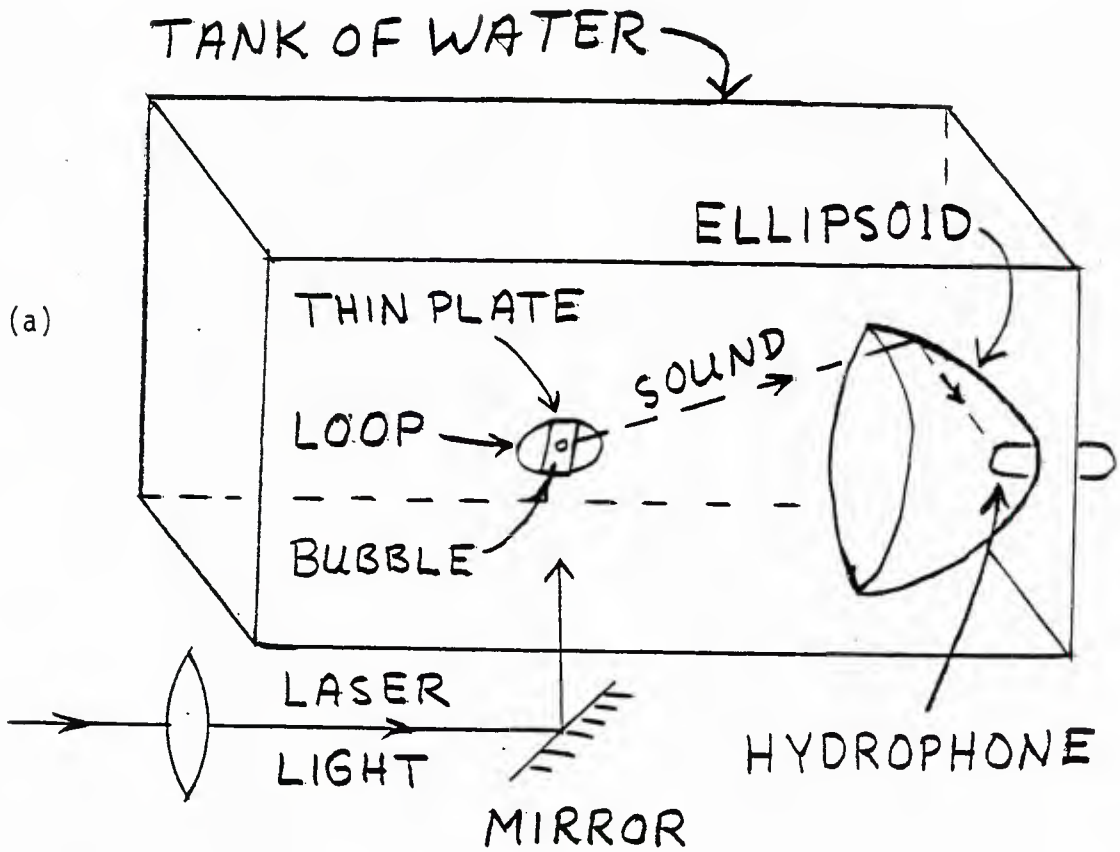
(a)
TANK OF WATER
ELLIPSOID
THIN PLATE
SOUND
LOOP
BUBBLE
LASER
LIGHT
HYDROPHONE
MIRROR

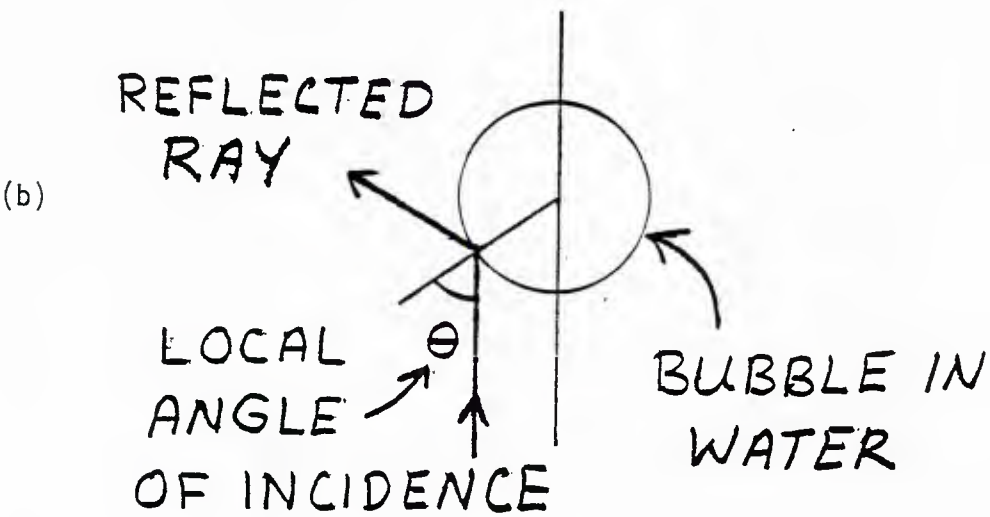
(b)
REFLECTED
RAY
LOCAL
ANGLE
OF INCIDENCE
θ
BUBBLE IN
WATER

Fig. 10

bubble's surface where the local angle of incidence θ, illustrated in Fig. 10(b), exceeds the critical value of $\theta_c = 48.6^o$ for total reflection from the bubble's surface. The reflection of light from the surface imparts a force which compresses the bubble and drives photo-acoustic mechanism (i) discussed in Sec. VA. Mechanism (ii), thermal expansion, should be small for this apparatus because of the optical absorption by the gas, surface, water, and substrate are all expected to be small (except perhaps, for the case of support by a hypodermic needle). Note that the irradiance minimum near the beam's center reduces the illumination in the region $\theta < \theta_c$. The beam power entering the bubble and then the substrate at the region where the bubble and substrate touch should be less than that power which either misses the bubble or is reflected from the bubble. We anticipate therefore that for support methods (2) and (3), mechanism (i) will dominate the production of sound.

To estimate the strength of the acoustic source, it is first necessary to average the radial (or compressive) projection of the radiation stress over the entire surface of the bubble. This average has been estimated by considering only the stresses due to the totally reflected portion of the beam and by approximating the incident wave as a plane wave having an irradiance I independent of θ. The resulting average pressure is[C1]

$$p_r \simeq FI, \quad F = (3c_L)^{-1} n_o \cos^3\theta_c, \tag{10a,b}$$

where $n_o = 1.33$ is the refractive index of water and c_L is the speed of light in a vacuum so that $F = 4.3 \times 10^{-10}$ s/m. The irradiance at the bubble's surface should have a magnitude $\simeq 2W/\pi(0.1\ \text{mm})^2 \simeq 6.4 \times 10^7\ \text{W/m}^2$. This value for I gives $p_r \simeq 0.027$ Pa (Pascals).

In the experiment, the irradiance I is modulated so that p_r depends on the time. To estimate the acoustic pressure amplitude p_A

radiated by the pulsating bubble it is convenient to take p_r to be a sinusoidal function of time

$$p_r(t) = p_{ro}[1 + \cos(2\pi ft)], \tag{11}$$

and to apply standard results from the theory of the scattering of a steady acoustic wave from a bubble. To apply these results p_{ro} takes on the role of the amplitude of an incident acoustic wave and we use the fact that the bubble radius $a \ll$ the acoustic wavelength in water $= c/f$. Then the modulus of p_A at a distance R from the bubble is predicted to be[26]

$$|p_A| = p_{ro}\, aG/R \tag{12}$$

where the function $G(f)$ has the following limiting forms[26]

$$\begin{aligned} G &\simeq (f/f_0)^2 \quad && \text{for } f \ll f_0 \\ G &\simeq Q && \text{for } f \simeq f_0\,, \\ G &\simeq 1 && \text{for } (c/2\pi a) \gg f \gg f_0. \end{aligned} \tag{13}$$

Here f_0 is the frequency for monopole resonance which for a free bubble is approximately given by[26]

$$f_0 \simeq \frac{1}{2\pi a}\left(\frac{3\gamma p_s}{\rho}\right)^{1/2} \simeq \frac{3300\ \text{kHz}}{a(\mu\text{m})}\,, \tag{14}$$

where ρ is the density of water, $p_s = 1$ atm is the static pressure, and $\gamma \simeq 1.4$ is the polytropic constant appropriate for either air or H_2 gas within the bubble. Instead of applying the results of scattering theory, Eq. (12)-(14) may be derived directly from bubble mechanics. For our size range

Figure 9 is a reproduction of Pearcey's original (1946) plot[17] of $|P(X,Y)|$. This, and other plots,[14] suggests that the amplitude near a directional cusp must be proportional to $P(X,Y)$ such that a horizontal scattering angle (relative to the cusp point in Fig. 3(b) of the Appendix) $\bar{\theta} = \theta - \theta_3$ and the vertical scattering angle ζ are locally linear in the arguments X and Y, respectively (θ_3 denotes the cusp point location and θ is the true horizontal scattering angle; see also Appendix I for a discussion of ζ.) The linear proportionalities $X \propto -\bar{\theta}$ and $Y \propto \zeta$ also follow from the number of stationary phase points in regions of $(\bar{\theta},\zeta)$ space partitioned by the caustic.[13,18] Unlike the form of Eq. (6), however, the far-field amplitude u at a distance r from the outgoing wavefront of amplitude $f(x,y)$ is given by a <u>two-dimensional</u> Fourier transform

$$u(\bar{\theta},\zeta) = \frac{2\pi}{i\lambda r} e^{ikr} F(\bar{\theta},\zeta) , \tag{7a}$$

$$F(\bar{\theta},\zeta) = \frac{1}{2\pi} \int_{-\infty}^{\infty} \int f(x,y) e^{-ik(\bar{\theta}x + \zeta y)} dxdy . \tag{7b}$$

This follows from scaler diffraction theory,[19] the Fraunhofer approximation, and the assumption that the angles $\bar{\theta}$ and ζ are each much smaller in magnitude than 1 radian; r is the distance of the observer from the origin 0 of the xy plane in which the complex amplitude $f(x,y)$ of the outgoing wave is specified. The direction defined by $\bar{\theta} = \zeta = 0$ lies perpendicular to the xy plane. The problem of finding the shape of the outgoing wavefront reduces to finding the form of $f(x,y)$ such that $F(\bar{\theta},\zeta) \propto P(X,Y)$ with $X \propto -\bar{\theta}$ and $Y \propto \zeta$.

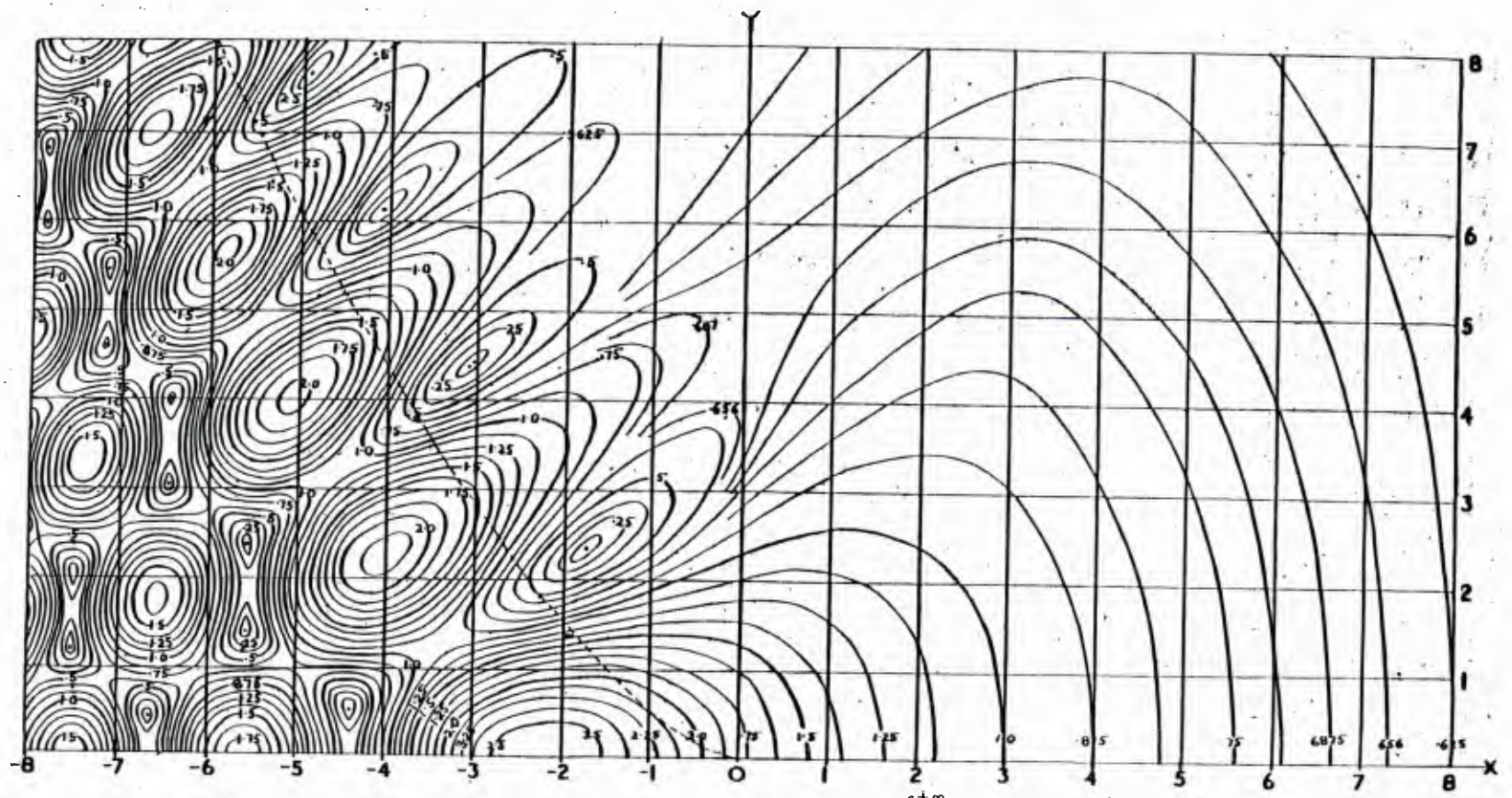

Contours of modulus of the cusp function $I(X, Y) = \int_{-\infty}^{+\infty} \exp i(Yt + Xt^2 + t^4)\, dt$.

Fig. 9

of bubbles the predicted[26] "quality factor" $Q \simeq 10$ and the predicted maximum value of $G \simeq Q$. To estimate the magnitude of the steady-state response at resonance we take $p_{ro} = 0.02$ Pa, a = 0.1 mm, R 100 mm, Q = 10 and Eq. (12) gives $|p_A| \simeq 0.0002$ Pa.

Because the magnitude $|p_A|$ of a freely spreading wave is estimated by Eq. (12) to be small, an ellipsoidal reflector was used to focus the acoustic emissions from the bubble onto the hydrophone. See Fig. 10(a). While focusing enhanced the sensitivity and made possible the detection of emissions from the bubble (stimulated by the low available optical powers), focusing complicates the measurement of acoustic source strength.

The procedure used in the experiments was as follows. A bubble was trapped and its diameter was measured with a microscope. The bubble was then illuminated by a rectangular pulse of light such that the pulse width T is less than $(2f_o)^{-1}$ as estimated from Eq. (14). It may be shown that the resulting $p_A(t)$ approximates the impulse response at a linear system where I(t) is the input and the bubble's acoustic emission $p_A(t)$ is the output. (If the long-time behavior of $p_A(t)$ is of interest it is also necessary to include the reverberations, of the emitted sound, from the walls of the chamber. These reverberations do not alter our interpretation of the experiments.) To obtain $p_A(t)$ with a satisfactory signal-to-noise ratio it was necessary to repeat this procedure and average the records obtained by using the Data Precision Digital Signal Processor. (Typically 256 records are averaged.) The resulting averaged impulse response $\bar{p}_A(t)$ is Fourier transformed by the signal processor via a FFT algorithm. This gives the frequency response g(f) of the bubble which should be proportional to the function G(f) in Eq. (12). The peak in the observed g(f) was measured to give an empirical resonance frequency f_{OE}.

The second stage of the experiment for each bubble was to demonstrate that bubble oscillations can be optically pumped at resonance to significantly increase the radiated amplitude $p_A(t)$. This was carried out by illuminating the bubble with a train of 4 pulses. The duration T of each pulse was adjusted to be $(2f_{OE})^{-1}$. The time separation between each pulse in the train was also taken to be T. Thus the modulating-spectrum of the illumination $I(t)$ was sharply peaked at the empirical resonance f_{OE}. To achieve a good signal-to-noise the emission $p_A(t)$ was repeatedly recorded. The resulting averaged resonance response $\bar{p}_A(t)$ had an initial increase in amplitude for 4 or 5 cycles followed by a decay. The maximum oscillation amplitude typically exceeded that of the impulse response, by a factor > 2. The observed p_A displayed the qualitative features expected for radiation by a resonator driven by a burst of pulses.

Figure 11 illustrates the signals obtained for a representative bubble with the configuration illustrated in Fig. 10(a). The measured bubble radius was 35 μm for which Eq. (14) gives $f_o \simeq 94$ kHz and $(2f_o)^{-1} \simeq 6$ μs. The bubble was then illuminated by single pulses of duration $T = 5$ μs and the averaged impulse response shown in Fig. 11(a) was obtained. (The vertical scale is the voltage output from a preamplifier/band-pass filter.) The FFT of this record was peaked at the empirical $f_{OE} = 77$ kHz. Figure 11(b) shows the averaged response to four pulses with a duration and spacing given by $T = (2f_{OE})^{-1}$ such that oscillations were forced at the frequency f_{OE}.

The leading edges of the signals in Fig. 11(a) and (b) are at 93 μs on the scale shown. These are close to the appropriate time allowing for propagation from the bubble to the hydrophone and other delays. On the scale shown, the bubble is first illuminated at 2.3 μs and there is an electronic group delay introduced by the preamplifier/band-pass filter of 2 μs so that

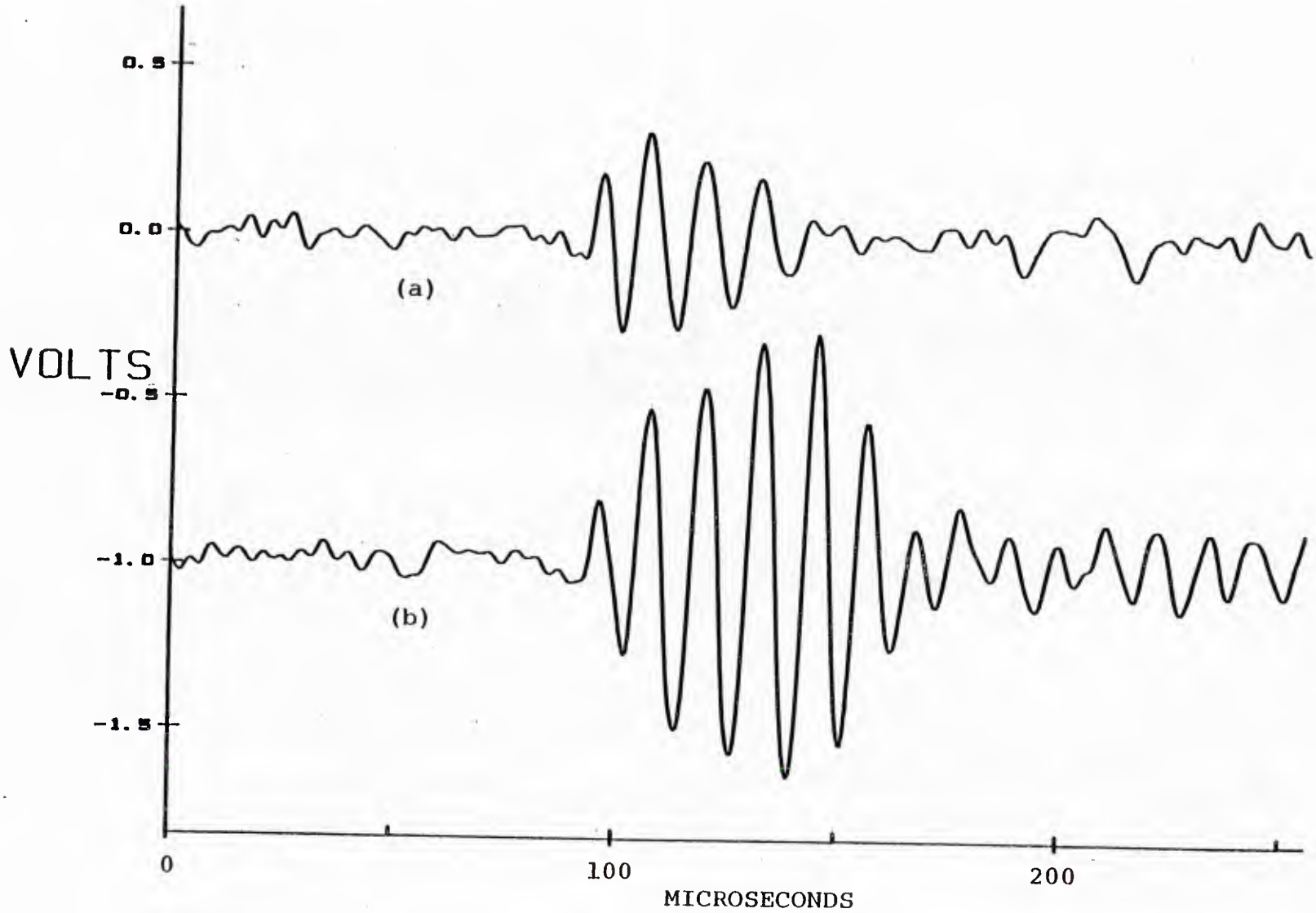

Fig. 11

the empirical propagation delay is 93-4 = 89 μs. The propagation distance in water for a signal via the ellipsoidal reflector is ~ 128 mm so the predicted delay is 128 mm/(1.49 mm/μs) = 86 μs. The observed signals clearly originate at the site of the bubble. However, in the absence of a bubble no signal is detected.

Figure 12 plots the measured values of natural frequency f_{OE} of a bubble as determined from the FFT of the averaged impulse response. These are plotted as a function of the measured reciprocal bubble radius a^{-1}. Also shown are the approximate natural frequencies given by Eq. (14), the dashed line, together with an improved approximation from Ref. 26 (which includes effects of surface tension and a reduction in the effective polytropic constant) that gives a lower predicted f_O. The observed natural frequencies are clearly close to those predicted for simple monopole oscillation of a bubble. Some comments on the discrepancies are in order: (i) The measured f_{OE}, as given by the peak in the FFT output, sometimes lies below the mean of the spectrum. For example, for Fig. 11(a), f_{OE} is 77.1 kHz while the spectral mean is closer to 80 kHz. (ii) The simple theories plotted do not include the shift in the downward natural frequency due to the support. Though this shift has been previously predicted to be small for bubbles supported by thin polymer films (e.g., the Mylar) it need not be negligible for bubbles supported by the thin glass plate.[27] (iii) For experiments done prior to April 17, 1985, there was sometimes a drift (reduction) in the size of the bubble during the recording of the averaged impulse response. This is to be expected for small bubbles as the gas dissolves. Subsequent to April the surrounding water has been saturated or supersaturated with dissolved gas (CO_2) to reduce the rate at which gas from the bubble goes into solution.

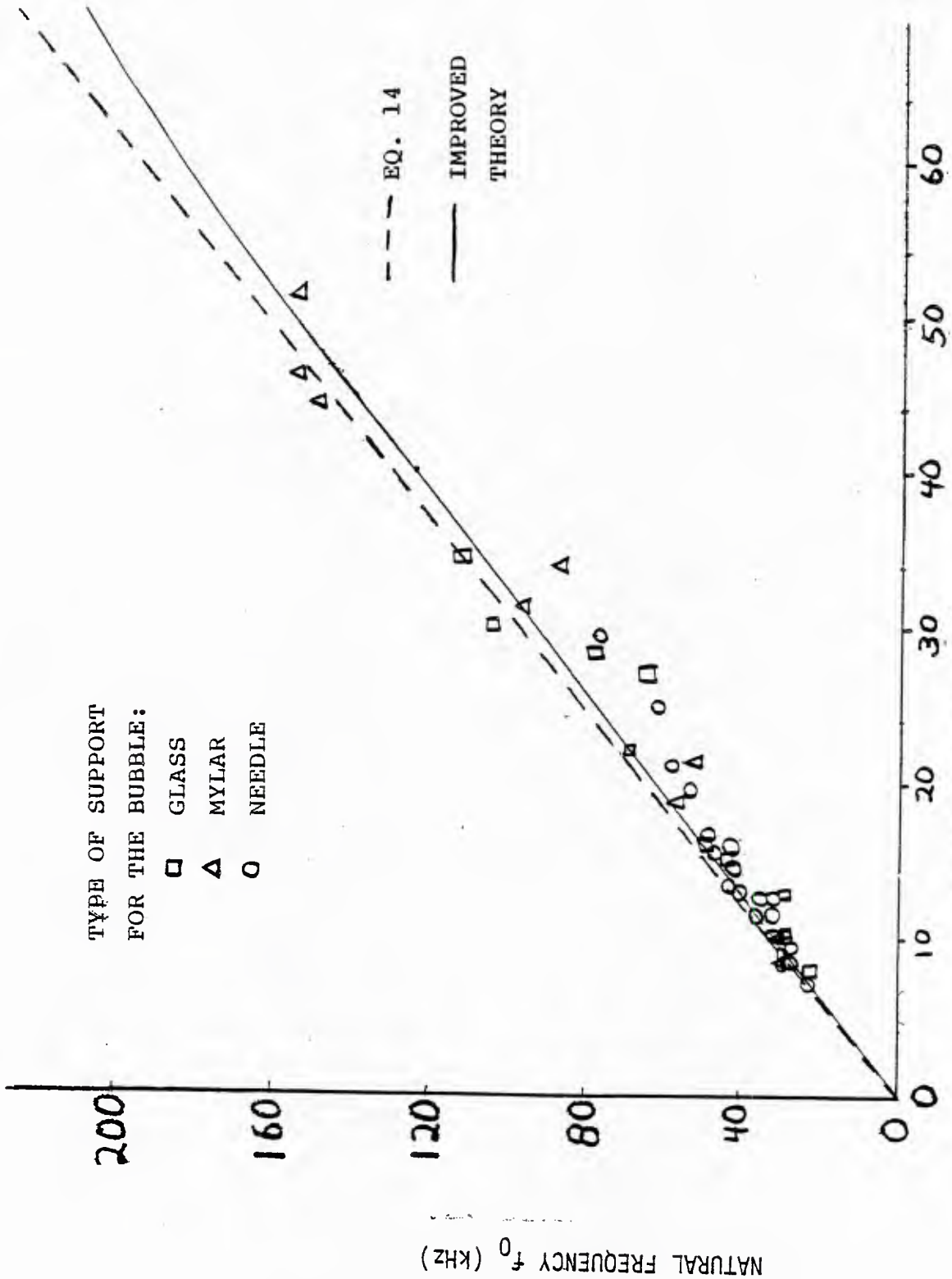
TYPE OF SUPPORT
FOR THE BUBBLE:
GLASS
MYLAR
NEEDLE
EQ. 14
IMPROVED
THEORY
NATURAL FREQUENCY f_0 (kHz)
(BUBBLE RADIUS (mm))$^{-1}$
0
40
80
120
160
200
10
20
30
40
50
60

Fig. 12

Much of the data shown in Fig. 12 was for illumination by a downward propagating light beam. Since April we have switched to the upward propagating beam as shown in Fig. 10(a) since the bubble emissions are easier to detect than in the downward propagating case. Evidently the surface of the bubble can be distorted close to the point of contact with the support. It is to be expected that this distortion would reduce the available area for total reflection from the bubble's surface in the case of a downward propagating beam but that it should have a negligible effect on the total-reflection area for the case of an upward propagating beam. Experiments are underway to further improve the reproducibility of the photo-acoustic signals as well as to indicate unambiguously the sign of the leading pressure fluctuation radiated by the bubble. Thereby we hope to clarify if the radiation pressure mechanism is indeed the dominant one as suggested by these observations.

During the course of these experiments we have also detected photo-acoustic emissions of dyed (or clear) drops of oils in water.

VI. Light Scattering from Bubbles in Water: Consideration of "Real" Versus "Ideal" Bubbles

A. Motivation for this Research and Review of Our Previous Research

This contract has previously supported research towards <u>understanding</u> the scattering of light from bubbles in liquids.[C1] A three-pronged approach has been used in these studies: (i) quantitative and qualitative observations and discovery of scattering phenomena; (ii) numerical evaluation of partial-wave series (such as the Mie series) which are for special bubble shapes (e.g., spheres) and comparison of these results with data; (iii) construction and evaluation of simple physical models which are both

the scattering pattern of freely rising bubbles in water to be essentially that of a sphere. Our previous visual observations (unpublished) showed that the backscattering or "glory" from sufficiently large bubbles in water deviated from the $(\sin 2\ )^2$ symmetry predicted for spheres. To quantify these effects and other reasons noted below, a graduate student, Pat Arnott, has been working with Marston to photograph for the first time the backscattering pattern from bubbles freely rising in water while simultaneously measuring their diameter D.

The measurement configuration used by Arnott is essentially that used in our previous work on glory scattering (see, e.g., Ref. D2, Fig. 1 of Ref. 32, or Fig. 2 of Ref. A10). The important differences are: (i) the illumination is now vertically-polarized light (from an Ar-Ion laser) having a wavelength $\lambda = 514$ nm and (ii) the bubbles rise freely in water through the scattering chamber, having been created on a needle about 10 cm below the chamber. Figure 13 shows representative photographs of the cross-polarized backscattering obtained as of September 1985. Figure 13(a) shows the scattering pattern for a bubble on water having $D \simeq 0.18$ mm. The dark vertical and horizontal bands (at $\varphi = 0^\circ$, 90°, 190°, and 270°) run through the center of symmetry (the backscattered direction) and are consequence of the predicted $(\sin 2\varphi)^2$ dependence and the dependence on the backscattering angle γ is similar to that expected for cross-polarized glory scattering. The pattern appears qualitatively to be that expected for a spherical bubble. Figure 13(b) shows the pattern for a bubble having $D \simeq 0.21$ mm and the pattern is again qualitatively that of a sphere. For bubbles which were sufficiently larger, there were clear deviations from the predicted $(\sin 2\varphi)^2$ symmetry as evident in Fig. 13(c) for a bubble having $D \simeq 0.40$ mm. These

deviations are clearly seen also in Fig. 13(d); which is for a bubble having $D \approx 0.34$ mm. Note that Figs. 13(a)-(c) are printed with common angular scale.

At present the available photographs suggest that deviations from sphericity do not qualitatively affect the scattering pattern if the bubble is smaller than about 0.30 mm diameter but that qualitative deviations are clearly evident for bubbles having diameters $\gtrsim$ 0.40 mm. For the size range studied the eccentricity of the bubble increases with the diameter. We hope to decrease the background noise evident in the photographs and to develop quantitative models of scattering from nonspherical bubbles in water.

It is appropriate to note that this problem may also be tied into our research on diffraction catastrophes (Sec. IV) because of suggestions[8,13] that the backward axially focused scattering from spherical objects (in this case bubbles) breaks-up into diffraction catastrophes when the axial symmetry of the scatterer is perturbed. In the terminology of catastrophe theory[13,14,18] we are studying the unfolding of the glory of a bubble in response to such perturbations.

C. Scattering of Light from a Coated Air Bubble in Water: A Computational Study of the Optical Effects of Adsorbed Films

As described in Sec. VA and VIA, bubbles in the ocean are thought to sometimes be coated by layers of surface active molecules. It is energetically favorable for such molecules to be situated at the air/water interface of the bubble instead of in the surrounding water. The effects of such molecules on bubble optics and acoustics are unclear. With the intent of studying this problem, Marston obtained in 1982 a computer program which could be adapted to give the optical scattering properties of coated bubbles. The partial-wave solution for electromagnetic scattering from a coated sphere

quantitatively useful and promote understanding. The general motivation for such research has been reviewed[8,C1] and we need only note here the following aspects:

1. The use of light scattering as a tool for studying bubbles in the ocean is on the increase. Such studies are important for several reasons:

   (a) Naturally-produced bubbles appear to affect the operation of high-frequency sonar systems.[28] The creation and evolution of such bubbles depends on the sea state; however, the detailed processes are not well understood.[24,28-30]

   (b) Such naturally produced bubbles are also important in physical and chemical oceanography since they affect the exchange of gas, sea salts, and other chemicals at the air-sea interface.

   (c) Since World War II, it has been known that wakes affect sound waves and that one of the significant causes appears to be bubbles trapped in the wake. It is not well understood why the bubbles appear to last for a long time; however, there has been recent speculation that adsorbed layers of surface-active molecules significantly reduce the rate at which the bubbles dissolve.[24,29]

2. Light scattering may prove to be a useful probe for studying the response of a bubble to sound waves. A quantitative discussion is given in Ref. B1 and C1 which is based in part on previous contract research.[31]

3. The detection and characterization of microbubbles is important in research on hydrodynamic as well as acoustic cavitation.[C1]

4. Microbubbles are used as tracers in hydrodynamics research.[C1]

5. The scattering of light from bubbles in the ocean[24b] may influence optical technologies for detection of (or communication with) submerged objects. The polarization properties of light scattered from bubbles may be particularly significant.[32,A10]

Our previous research has continued to be used by other researchers[30] for interpreting data on the population spectra obtained by optical means. It appears worthwhile, however, to explore certain "real" bubble phenomena not included in our previous models of "ideal" bubbles (spherical bubbles having clean surfaces).

B. Observations of Optical Backscattering from Freely Rising Bubbles in Water: The Unfolded Glory of an Oblate Bubble

The cross-polarized near-backward and near-forward irradiance I_S scattered from spheres has a predicted dependence on azimuthal angle φ of the form:[32,A10] $I_S \propto (\sin 2\varphi)^2$. The incident light is assumed to be linearly polarized. This is in qualitative agreement with the observed azimuthal symmetry of backscattering from air bubbles in a viscous silicone oil which should be nearly perfect spheres. On the other hand, freely rising bubbles in water are subjected to hydrodynamic stresses which deform bubbles into a shape closely resembling that of an oblate spheroid[31] with a vertical axis of rotational symmetry. For illumination by horizontally propagating light, our measurements of near critical-angle scattering in the horizontal plane show

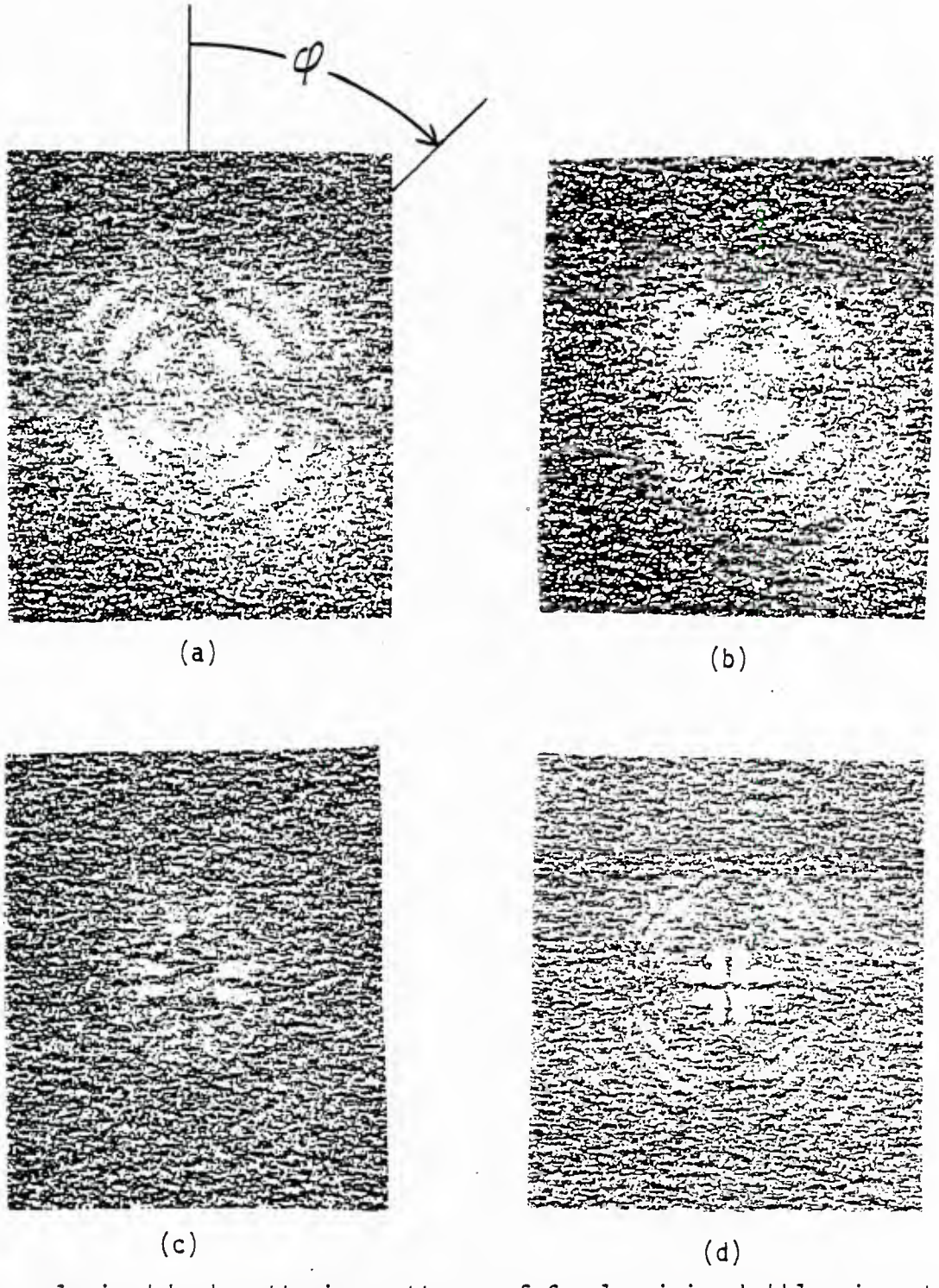

Cross-polarized backscattering patterns of freely-rising bubbles in water. The definition of the azimuthal angle φ is shown. The backscattering angle γ is proportional to the distance from the center of the pattern.

Fig. 13

is known[33] and this program numerically evaluates that series. Unfortunately, hitherto the resources were not adequate to complete the testing of this computer algorithm. A graduate student, Stuart Billette, is presently working on this problem. It is our intent to compute how thick the film needs to be (for a range of refractive indices) for the scattering from bubbles in water to be significantly affected by the coating. Light scattering may prove to be a useful diagnostic tool for in situ measurements of the film thickness on bubbles in water.

D. Forward-Optical Glory of Bubbles in Silicone Oil and in Water and Near-Forward Scattering Properties of Bubble Clouds

A brief description of our previous research[C1,C2] on these topics has been submitted for publication.[A10] This includes photographs of the cross-polarized forward optical glory pattern of a bubble in silicone oil having a diameter of 0.25 mm and of a bubble cloud in water. D. S. Langley (who presently teaches at Whitman College, Walla Walla, WA) is preparing a detailed manuscript on this research.

VII. Other Research

Other previous research, supported partially by O.N.R., which was published or submitted for publication includes: (i) calculations of the radiation torque[A2] and angular momentum of the scattered field[A11] for spheres illuminated by circularly polarized light; (ii) research on the oscillation and break-up of oil drops in water stimulated by the modulated radiation pressure of high-frequency sound;[4] and (iii) experiments which demonstrated rapid cavitation in water (and in ethelene glycol) which resulted from the reflection of a shock pulse (of duration < 2 μs) from a free liquid surface.[A8,C1]

VIII. References

1. L. R. Dragonette, S. K. Numrich, and L. J. Frank, "Calibration technique for acoustic scattering measurements," J. Acoust. Soc. Am. 69, 1186-1189 (1981).

2. L. Flax, L. R. Dragonette, and H. Uberall, "Theory of elastic resonance excitation by sound scattering," J. Acoust. Soc. Am. 63, 723-731 (1978).

3. L. Flax, G. C. Gaunaurd, and H. Uberall, "Theory of resonance scattering," in Physical Acoustics, edited by W. P. Mason and R. N. Thurston (Academic, New York, 1981), Vol. 15, pp. 191-294.

4. G. C. Gaunaurd and H. Uberall, "RST analysis of monostatic and bistatic acoustic echoes from an elastic sphere," J. Acoust. Soc. Am. 73, 1-12 (1983).

5. See e.g. Eq. (46c) of Ref. 3.

6. L. Flax, "High ka scattering of elastic cylinders and spheres," J. Acoust. Soc. Am. 62, 1502 (1977).

7. P. L. Marston and D. S. Langley, "Glory in backscattering: Mie and model predictions for bubbles and conditions on refractive index in drops," J. Opt. Soc. Am. 72, 456-459 (1982).

8. P. L. Marston, "Proposal on Propagation and Effects of Acoustical and Optical Waves," for renewal of contract N00014-80-C-0838 (submitted to ONR Code 412 in September 1984).

9. I. Tolstoy, "Scatter from a rough surface," J. Acoust. Soc. Am. 72, 973-975 (1982).

10. R. Hickling, "Analysis of echoes from a hollow metallic sphere in water," J. Acoust Soc. Am. 36, 1124-1137 (1964).

11. M. C. Junger and D. Feit, "High-frequency response of point-excited submerged spherical shells," J. Acoust. Soc. Am. 45, 630-636 (1969).

12. J. F. Nye, "Rainbow scattering from spheroidal drops: an explanation of hyperbolic-umbilic foci," Nature (London) 312, 531-532 (1984).

13. M. V. Berry, "Waves and Thom's theorem," Advances in Physics 25, 1-26 (1976).

14. M. V. Berry and C. Upstill, "Catastrophe optics: Morphologies of caustics and their diffraction patterns," Prog. Opt. 18, 257-346 (1980).

15. R. L. Holford, Modifications to ray theory near cusped caustics in Contract Report (Bell Laboratories, Whippany, NJ, 1972).

16. G. Dangelayr and W. Guttinger, "Topological approach to remote sensing," Geophys. J. R. Astr. Soc. 71, 79-126 (1982).

17. T. Pearcey, "The structure of an electromagnetic field in the neighbourhood of a cusp of a caustic," Phil. Mag. 37, 311-317 (1946).

18. R. Gilmore, Catastrophe Theory for Scientists and Engineers (Wiley, New York, 1981).

19. J. W. Goodman, Introduction to Fourier Optics (McGraw Hill, New York, 1968).

20. J. F. Nye and J. H. Hannay, "The orientations and distortions of caustics in geometrical optics," Optica Acta 31, 115-130 (1984).

21. V. I. Arnold, Singularity Theory (U.P., Cambridge, 1981).

22. R. Gilmore, Lie Groups, Lie Algebras, and Some of Their Applications (Wiley, New York, 1974).

23. W. Lauterborn and K. J. Ebeling, "Highspeed holography of laser-induced breakdown in liquids," Appl. Phys. Lett. 31, 663-664 (1977).

24. (a) R. E. Glazman, "Damping of bubble oscillations induced by transport of surfactants between the adsorbed film and the bulk solution," J. Acoust. Soc. Am. 76, 890-896 (1984).

(b) V. V. Goncharov et al., "Determination of the diffusion constant of a gas bubble in sea water from the solution of air bubbles in the medium," Soviet Physics Acoustics 30, 273-25 (1984).

25. "The sound of air bubbles," Science News 127, 281 (1985).

26. C. S. Clay and H. Medwin, Acoustical Oceanography Principles and Applications (Wiley, New York, 1977) pp. 194-203.

27. J. E. Ffowcs Williams and W. F. Hunter, "The scattering of multipole near-field sound by a gas bubble," Proc. Roy. Soc. Lond. A314, 363-385 (1970).

28. E. I. Thorsos, Surface Forward Scattering and Reflection (Report No. APL-UW7-38, Applied Physics Laboratory, University of Washington, Seattle, 1984).

29. S. A. Thorpe, "On the clouds of bubbles formed by breaking wind-waves in deep water, and their role in air-sea gas transfer," Phil. Trans. R. Soc. Lon. A304, 155-210 (1982).

30. S. Baldy and M. Bourguel, "Measurements of bubbles in a stationary field of breaking waves by a laser-based single-particle scattering technique," J. Geophys. Res. 90C, 1037-1047 (1985).

31. D. S. Langley and P. L. Marston, "Critical-angle scattering of laser light from bubbles in water: measurements, models, and application to sizing of bubbles," Applied Optics 23, 1044-1054 (1984).

32. P. L. Marston and D. S. Langley, "Strong backscattering and cross-polarization from bubbles and glass spheres in water," Ocean Optics VI, Proc. of the Soc. of Photo-Optical Instrumentation Engineers 489, 130-141 (1984).

33. A. L. Aden and M. Kerker, "Scattering of electromagnetic waves from two concentric spheres," J. Appl. Phys. 22, 1242-1246 (1951).

APPENDIX 1:

(Accepted for publication in Optics Letters)

Cusp diffraction catastrophe from spheroids: generalized rainbows and inverse scattering

Philip L. Marston

Department of Physics, Washington State University

Pullman, Washington 99164

(abstract)

The angular location of the recently discovered cusp pattern in the far-field scattering from an oblate spheroid is calculated as a function of the aspect ratio D/H. The calculation assumes the diameter $D \gg \lambda$ and is limited to illumination perpendicular to the short axis of the spheroid. It agrees with observations for water drops in the range $1.22 < D/H < 1.37$ with $D \sim 1$ mm.

PACS Nos. 42.10.Hc, 42.20.Gg, 03.80.+r

The scattering from spheroidal drops of water into the rainbow region was recently observed to manifest hyperbolic-umbilic and cusp diffraction catastrophes not previously known to appear.[1] In the present letter, the angular location of the cusp is calculated as a function of the axis ratio of an oblate spheroid. This calculation is compared with previously unreported data and applications of these phenomena to a restricted class of inverse scattering problems are noted. As in the original paper,[1] the emphasis of this letter is on illumination by a monochromatic plane wave with a wavelength λ which is much smaller than the drop. The conditions under which a cusped rainbow might be observed in nature, as a result of solar illumination of rain, will also be considered.

The scattering patterns observed are a generalization[1,2] of the primary rainbow formed by a spherical drop.[3-5] The scattering is enhanced near foci where the amplitude diverges unphysically according to geometrical optics.[5] Catastrophe theory[5-8] classifies foci and removes these divergences by introducing canonical diffraction integrals. The classification is in terms of diffraction catastrophes; the rainbow of a sphere is a manifestation of a fold diffraction catastrophe. Like the rainbow, the novel catastrophes for the spheroid are examples of angular or far-field foci (though the foci are not confined to the far field). Near focal angles, the scattering amplitudes are large and the patterns may be useful for characterizing the scatterer. Umbilic near-field foci have been observed in the light transmitted by liquid lenses (on glass plates) or reflected from curved surfaces.[5-7]

The scatterer to be considered is a water drop whose shape closely approximates that of an oblate spheroid with the short axis (the symmetry axis) vertical. In the experiments, the drops were illuminated by a horizontally propagating (and randomly polarized) Gaussian beam with

$\lambda = 633$ mm. The drop's diameter will be denoted by D in the horizontal equatorial plane P, and by H along the vertical axis. The beam diameter greatly exceeded D and the incident wave approximated a plane wave. Rays which are incident on the equator are confined to P. The relevant rays are the once-reflected (twice-refracted) rays shown in Fig. 1. They have a minimum scattering angle of $\theta_R \simeq 138^\circ$ which is the scattering angle of the Descartes ray.

The experimental apparatus is described in Ref. 1 and will be reviewed here. An ultrasonic standing wave in air was used both to levitate the drop and to control its axis ratio $q = D/H$. The oblate shape is due to the spatial distribution of the acoustic radiation pressure. The ultrasonic wave was vertically directed; raising its amplitude increases q. The scattering was photographed by a camera focused on infinity. The pattern recorded was equivalent to the angular distribution of the irradiance in the far-field (which is at distances $r >> D^2/\lambda$ from the drop). Horizontal and vertical coordinates in each photograph were linear in the horizontal and vertical scattering angles θ and ζ, where ζ is measured relative to plane P. A second camera, focused on the drop, facilitated the measurement of D and H.

In the following discussion of the qualitative features of the scattering, it will be convenient to use Arnold's symbols A_2, A_3, and D_4^+ to designate[8] fold, cusp, and hyperbolic-umbilic diffraction catastrophes, respectively. For q sufficiently close to unity, an A_2 pattern is observed consisting of supernumerary arcs described by Airy theory for the dominant polarization.[4] Increasing q shifts an A_3 pattern into view in the region for large θ scattering; also the arcs of the A_2 pattern become noticeably bent. Figure 2(a) shows this scattering pattern for a drop having $q \simeq 1.23$ and $D = 1.39$ mm. For q at (or very close to) a critical value

measured[1] to be 1.305 ± 0.016, the pattern in Fig. 2(b) is observed. This corresponds to the focal section of a D_4^+ pattern. Further increases in q cause the pattern to separate back into A_2 and A_3 patterns. Figure 2(c) shows this pattern for a drop having $q \simeq 1.37$ and $D = 1.40$ mm. The θ of the Descartes ray in P does not depend on q. Consequently the location of the left-most fringe in the A_2 patterns (visible eq. in Fig. 2(a) and (c)) are observed to be nearly independent of q. In the region close to $(\theta,\zeta) = (\theta_R,0)$, patterns with q close to that of the focal section display features expected of D_4^+ diffraction patterns.[1] The A_3 pattern, when well separated from θ_R, displays the features expected from the canonical A_3 diffraction integral which is the Pearcey integral.[7,9]

The D_4^+ catastrophe occurs because there are two once-reflected (twice-refracted) rays which are <u>not confined to</u> P but which merge with the Descartes ray when q takes on the critical value of[2] $q_4 = [3\mu^2/4(\mu^2 - 1)]^{1/2} \simeq 1.311$, where the refractive index μ of the drop is 1.332. This is in agreement with the aforementioned measurement. The two new rays, which may be classified as <u>skew rays</u>,[10] were first noticed from photographs[1] <u>of the drop</u> taken with a camera whose aperture lay near P at a scattering angle $> \theta_R$. Figure 3(a), drawn from such a photograph, shows the locations of the rays as they leave the drop. Rays 1 and 2 correspond to those in Fig. 1. The existence of the skew rays is consistent with there being up to four stationary points of the phase function within the D_4^+ diffraction integral.[5,8] With $q \neq q_4$, the scattering pattern may be partitioned into three regions giving the number of nondegenerate stationary-phase points of the diffraction integral. These give the number of rays which propagate to each region as shown in Fig. 3(b). Equatorial rays (or their generalization for $\zeta \neq 0$) are present in the two-ray region.

Three rays merge in the direction of the cusp point.[5] For the problem under consideration these consist of two skew rays and one equatorial ray. This focal direction is $(\theta,\zeta) = (\theta_3,0)$ where θ_3 is related to q by the calculation which follows. First consider an equatorial ray scattered toward θ. Let the first to two vertices for this ray be denoted by points U and U' in plane P (Fig. 1). The angles of incidence and refraction at U will be denoted by i and r, respectively. Snell's law gives $\sin i = \mu \sin r$ and geometry gives $\theta(i,r) = 180^\circ - 4r + 2i$. Now consider an incident ray parallel to the ray incident at U, but displaced vertically from it by a small distance ε. The first vertex of this skew ray is at $\underset{\sim}{v}$ where the origin of the coordinate system is the center C of the circle in P. The z axis is vertical giving $v_z = \varepsilon$. The scattered skew ray has $\zeta = O(\varepsilon)$ except when $\theta = \theta_3$ in which case $\zeta = O(\varepsilon^3)$. Through terms of $O(\varepsilon^2)$, the skew ray is directed horizontally <u>after leaving the drop</u> if the incident ray lies above the equatorial ray having $\theta = \theta_3$. This skew ray, when in the drop, reflects at a vertex at $\underset{\sim}{v}'$ which coincides with U' except for residual $O(\varepsilon^2)$ terms. (The argument also applies to the skew ray incident below plane P.) A related argument was introduced by Nye[2] in his derivation of q_4. Let $\underset{\sim}{n}$ be a unit vector directed along the refracted skew ray between $\underset{\sim}{v}$ and $\underset{\sim}{v}' = \underset{\sim}{v} + \Lambda \underset{\sim}{n}$; Λ, $\underset{\sim}{v}$, and $\underset{\sim}{n}$ may be computed using Herzberger's formalism.[10] The aforementioned condition that $v_z'/\varepsilon \to 0$ as $\varepsilon \to 0$ gives the following condition linking q with $S = \sin^2 i$ of the associated equatorial ray:

$$q = \mu[2w'(w' - w)]^{-\frac{1}{2}}, \quad w' = (\mu^2 - S)^{\frac{1}{2}}, \tag{1}$$

where $w = (1-S)^{\frac{1}{2}}$ and $\theta_3 = 180^\circ + 2i - 4 \sin^{-1}(S^{\frac{1}{2}}/\mu)$ give a parametric representation of $q(\theta_3)$. A coplanarity condition discussed by Nye[2] equivalently yields (1).

Figure 4 shows the resulting $q(\theta_3)$ obtained by taking i as a parameter which runs from 0°, giving point L, to 90°, giving T. The usual rainbow condition, $S = (4 - \mu^2)/3$, gives $\theta_3 = \theta_R$ and $q = q_4$. To test the calculation, $(\theta_3 - \theta_R)$ was estimated from photographs of the scattering pattern. Plots of the Pearcey integral[9,11] show that the cusp point location θ_3 is less than the θ of the irradiance maximum because of diffraction. A line drawn close to the outermost discrete nulls of the Pearcey integral crosses the cusp. This procedure was adapted here so that $(\theta_3 - \theta_R)$ could be estimated in the absence of densitometer scans. Figure 2(a) and (c) give $(\theta_3 - \theta_R)$ of 5.0° and 4.1°, respectively. A photograph of the drop's profile was recorded within a few seconds of the diffraction pattern. Experience with the measurement[1] of q_4 shows that even with a well defined condition and several photographs, there is a substantial uncertainty in the measurement of q. This appears in part to be a consequence of drift in the levitation position of the drop and because of the continual evaporation of the drop. The error bars on the data for each pair of photographs were estimated from the experience with q_4, comparison with other profile photographs in a sequence (when available), and the magnitude of λdependent corrections not incorporated in the estimates of θ_3. Systematic uncertainties may also be present since the incident beam may not be exactly horizontal and the drops are not perfect spheroids. The measurements evidently confirm the calculation.

As $i \to 90^\circ$, Eq. (1) gives $q \to q_T = \mu(2\mu^2 - 2)^{-\frac{1}{2}} \simeq 1.070$ and $\theta \to \theta_T \simeq 166^\circ$. This is a Fock-type transition[3] for the ray labeled 1 in Fig. 1; Fresnel coefficients lead to the incorrect prediction that the scattering amplitude associated with this ray vanishes as $i \to 90^\circ$. The branch of θ_3 for the region $q_T < q < q_4$ locates the merging of the rays labeled 1, 3, and

4 in Fig. 3(a). As $i \to 0^{\circ}$, Eq. (1) gives $q \to q_L = [\mu/(2\mu - 2)]^{\frac{1}{2}} \simeq 1.416$ and $\theta \to 180^{\circ}$ which is Nye's predicted lips event.[2] The branch of θ_3 for the region $q_4 < q < q_L$ locates the merging of the rays labeled 2, 3, and 4 in Fig. 3(a). The merging of skew rays with either of rays 1 and 2 was confirmed from photographs of drops. For a given angular location of the camera's aperture, the values of q which produced a merging of rays were consistent with Eq. (1). See Fig. 5.

Diffraction integrals[5] applied to this scattering problem lead to the following scaling laws for the irradiance I at the focal angles of A_2, A_3, and D_4^+ catastrophes: $I \propto (D/\lambda)^p (D/r)^2$ where q is fixed and $p = 1/3$, 1/2, and 2/3, respectively. Experimentally, the foci listed in the order of increasing apparent exposure are A_2, A_3, and D_4^+ which is in qualitative agreement. For the inverse problem of determining q, measurements of $(\theta_3 - \theta_R)$ may be useful even if D is not well known since θ_3 is independent of $D \gg \lambda$. In principle, D may be determined from the widths of the diffraction structures near the foci (for the scaling laws see Ref. 5) or from the value of I. The A_3 and D_4^+ patterns may be used as benchmarks for testing algorithms[12] for the scattering.

Freely falling raindrops have an oblate shape. If the sun is very near the horizon, they might exhibit an A_3 focus or "cusped rainbow" in addition to the usual A_2 rainbow. The drops need not be exact spheroids since the principal curvatures at the equator determine θ_3. The D/H of raindrops increase with D; models cited in Ref. 1 suggest that a drop with $D/H \simeq q_T$ has $D \simeq 1.8$ mm. For the A_3 focus to be visible it may be necessary to have $D > 1.8$ mm. Drops in a shower will have a distribution of effective q and dispersion causes θ_3 to depend on λ as well as q.

This research was supported by the Office of Naval Research. The experiments were carried out during a visit to the Microgravity Science and Applications Laboratory (supported by NASA) of Jet Propulsion Laboratory.

References

1. P. L. Marston and E. H. Trinh, Nature (London) 312, 529 (1984).

2. J. F. Nye, ibid. 312, 531 (1984).

3. H. M. Nussenzveig, J. Math Phys. (N.Y.) 10, 125 (1969).

4. G. P. Können and J. H. deBoer, Appl. Opt. 18, 1961 (1979).

5. M. V. Berry and C. Upstill, Prog. Opt. 18, 257 (1980).

6. R. Thom, Stabilité structurelle et morphogénèse (Benjamin, Reading, Mass., 1972).

7. M. V. Berry, J. F. Nye, and F. J. Wright, Philos. Trans. R. Soc. London, A291, 453 (1979).

8. V. I. Arnold, Singularity Theory (U.P., Cambridge, 1981).

9. T. Pearcey, Philos. Mag. 37, 311 (1946).

10. M. Herzberger, Modern Geometrical Optics (Interscience, New York, 1958).

11. The two-dimensional diffraction integral reduces to Pearcey's integral with an integrand $\exp[is^4 + is^2(\theta-\theta_3)a_2 + is\zeta a_1]$ and an integration variable $s = a_0\varepsilon$; the a_j are functions of D, H, λ, and μ.

12. S. Asano and G. Yamamoto, Appl. Opt. 14, 29 (1975).

Figure Captions

Fig. 1. Rays through a spheroidal drop in the horizontal equatorial plane.

Fig. 2. Photographs of the scattering into the rainbow region. The horizontal scattering angle θ increases from left to right. The axis ratio D/H of the drops increases from (a) to (c).

Fig. 3.(a) Locations of once reflected (twice-refracted) rays as they leave a drop. (b) Partitioning of a scattering pattern with $D/H \neq q_4$.

Fig. 4. The dependence of D/H on the cusp location θ_3. The prediction is the curve and the ● are measurements. ▲ is the measured q_4 from Ref. 1.

Fig. 5. Drops having D/H of (a) 1.21 and (b) 1.14. The camera's aperture is at $\theta \approx 143^\circ$ which is close to θ_3 for (a) but is well inside the two-ray region for (b). Ray 1 is visible near the left edge of each drop however in (a) skew rays merging with it form a bright arc. The bright patch near each center is not related to the laser illumination. It is from the diffuse source used to highlight the profiles.

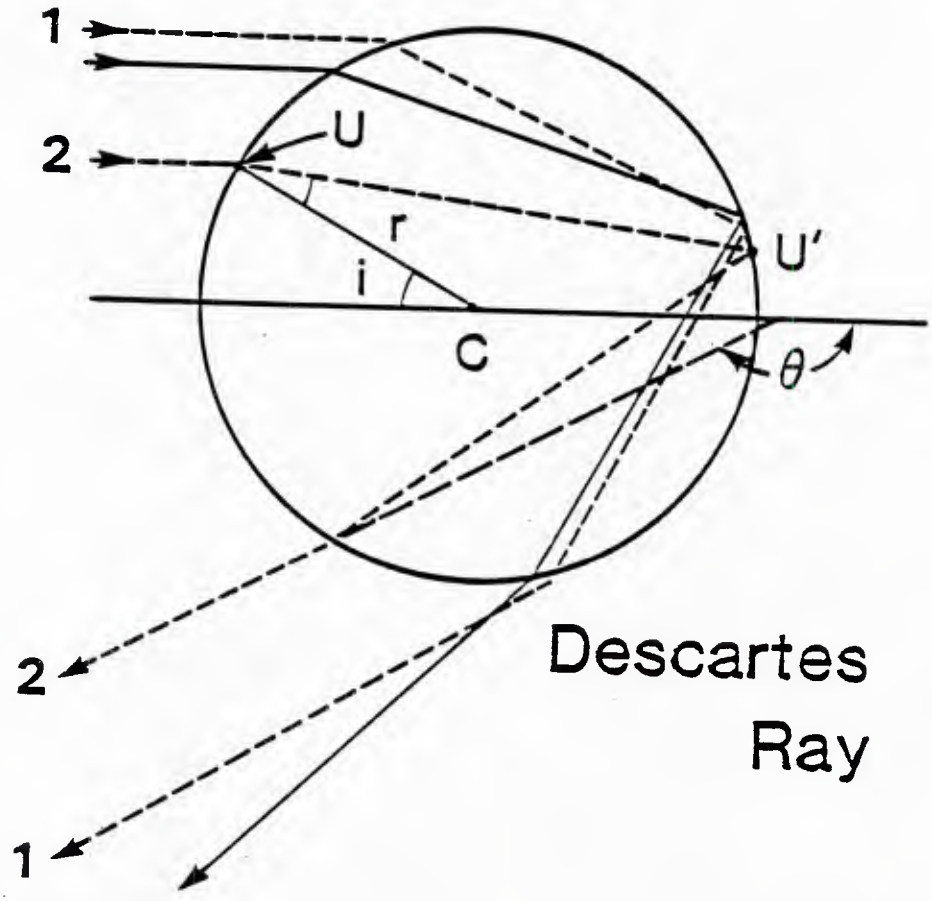

Fig. 1

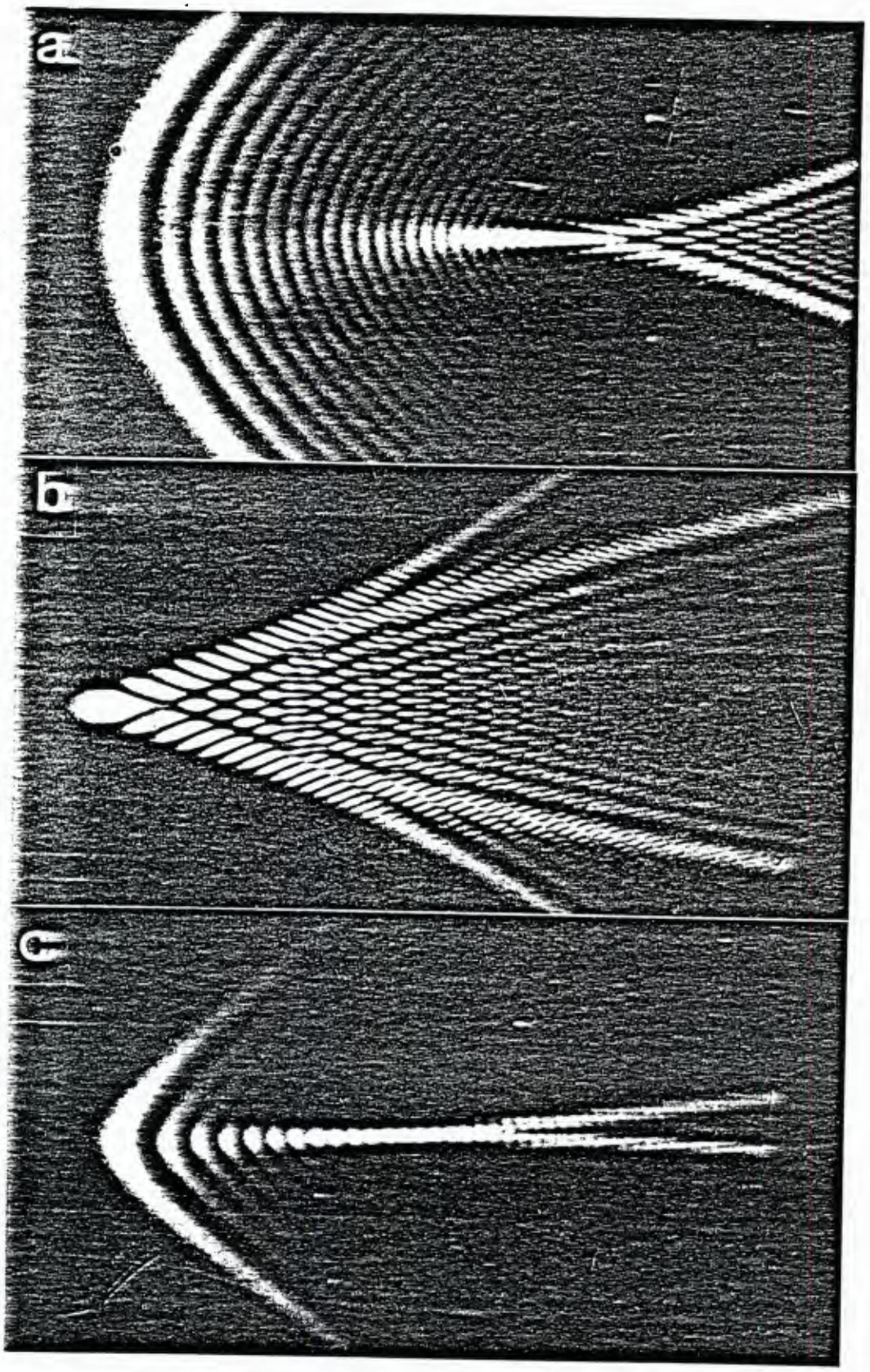

5 deg

Fig. 2

Fig. 3

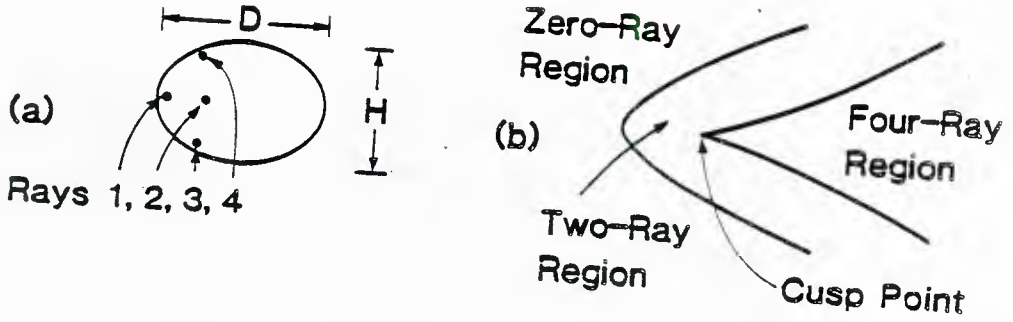

Fig. 4

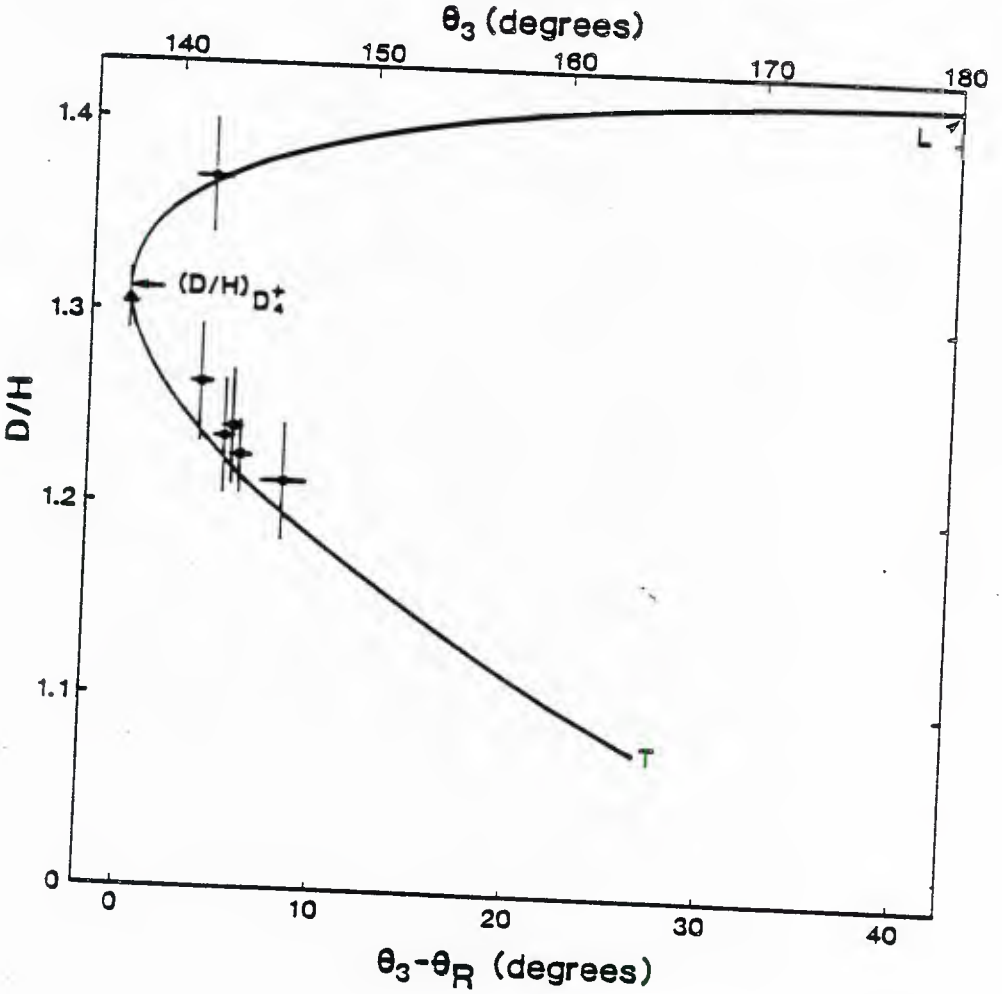

Fig. 5

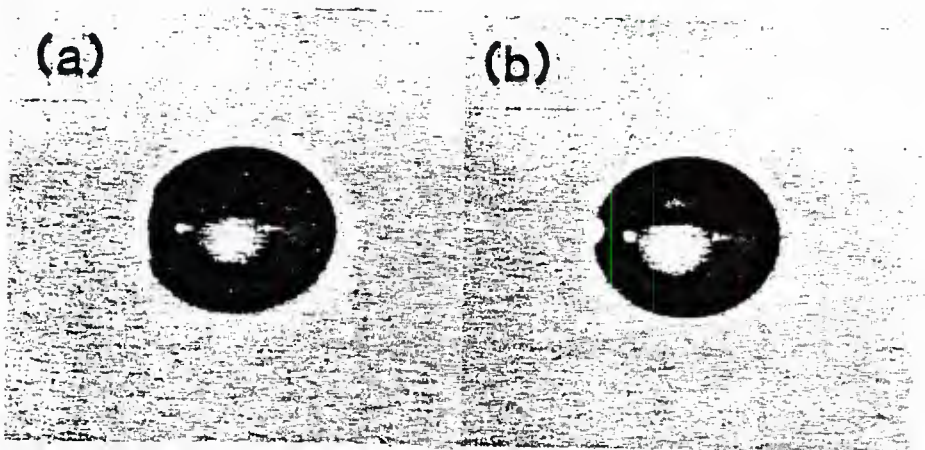

APPENDIX 2:

AIP news release

American Institute of Physics, 335 East 45th Street, New York, N.Y. 10017 • TELEPHONE (212) 661-9404
Telex 960983/AMINSTPHYS-NYK

Public Information Division
David A. Kalson, Manager

NOTE TO EDITORS: Press inquiries during the 109th Meeting of the Acoustical Society of America, being held April 8-12, 1985, can be directed to Harry D. Record at Tracor Applied Sciences in Austin, Texas (Telephone: 512-929-2040).

RELEASED FOR SATURDAY MORNING, APRIL 13, 1985

Authors' Popular Version of Paper: UU-7

"OPTICALLY STIMULATED SOUND FROM GAS BUBBLES IN WATER: A NOVEL OPTOACOUSTIC MECHANISM"

Presented by: Bruce T. Unger and Philip L. Marston
Department of Physics
Washington State University
Pullman, Washington 99164

Optically Stimulated Sound from Gas Bubbles in Water: A Novel Optoacoustic Mechanism*

Bruce T. Unger and Philip L. Marston
Department of Physics
Washington State University
Pullman, Washington 99164

Sound is produced when intense light is absorbed by matter. This effect was discovered in the 1880's by Alexander Graham Bell, Wilhelm Rontgen, and John Tyndall. The phenomena of generating sound from light has become known as the optoacoustic (or photoacoustic) effect. Interest in this effect has grown rapidly since about 1970 as modulated laser light became widely available to researchers. The optoacoustic effect is frequently used to study the wavelength dependence of the absorption of light by gases, liquids, and solids. The common physical mechanism in these applications is the heating of matter which is the consequence of the absorption of light. The local temperature increase causes an expansion of the material. The illumination is modulated in time so that the material alternately expands and contracts generating sound waves which propagate outward from the heated region.

The novel result of our research is that small gas bubbles in water produced sound when illuminated by modulated laser light. Prior to describing this research, it is appropriate to review some properties of bubbles in water. Bubbles in the ocean are known to be effective scatterers of high frequency sound. This scattering of sound has been used to study clouds of bubbles which are produced when waves break on the ocean's surface. It is also known that when a bubble vibrates, so that its volume oscillates, sound is radiated from the bubble into the surrounding water. The radial oscillations of a bubble are analogous to the vibrations of a mass attached to

---

*Research supported by the U.S. Office of Naval Research.

a coiled spring. The water outside the bubble provides the inertia while the gas within impedes compression and acts like a spring. The generation and scattering of sound are most effective when the frequency corresponds to the natural pulsation frequency of the bubble, A bubble with a radius of 0.1 mm has a natural frequency of about 30 kHz.

The physical processes associated with the scattering of light from bubbles are being investigated at Washington State University. The ways in which light is scattered from bubbles in water are different than the ways it is scattered from drops of rain. For example, light is nearly totally reflected from parts of the surface of a bubble.

The aforementioned optical and acoustical properties led us to propose that bubbles radiate sound when illuminated by pulsed laser light. Light carries momentum and the reflection of light at any surface imparts a force to that surface. This force or "radiation pressure" on the surface of a bubble is enhanced by the high reflectivity. The radiation pressure pushes and compresses the bubble so as to reduce its volume. When the light is modulated, the bubble should alternately contract and expand, thereby radiating sound. Unlike the usual optoacoustic effect, expansion need not be caused by heating and cooling.

We have recently detected optically stimulated sound from gas bubbles. Single bubbles in clear water were attached either to a needle or to a thin film of transparent Mylar. The radius of the bubble was typically smaller than 0.1 mm. The sounds radiated by these bubbles were reflected from a curved metal surface and were focused on a hydrophone (a microphone designed to operate in water). The bubbles were illuminated with light pulses having a peak power of about 2 watts. The sound detected by the hydrophone exhibited oscillations at the natural frequency of the bubble. The arrival time of this

signal is further evidence that the bubble was the source of the sound: the signal was delayed by a time appropriate for propagation of sound from the bubble to the hydrophone. Bubbles were subsequently illuminated by bursts of light pulses with a frequency corresponding to the observed natural frequency. The resulting sound was characterized by an initial build-up of its amplitude. This is the expected response of a forced oscillator.

Depending on the bubble's environment, radiation pressure may not be the only cause of the optoacoustic effect of bubbles. Absorption and heating may also be significant and further investigations are in progress to elucidate the physical processes involved.

APRIL 1984

REPORTS DISTRIBUTION LIST FOR ONR PHYSICS DIVISION OFFICE
UNCLASSIFIED CONTRACTS

Director
Defense Advanced Research Projects Agency
Attn: Technical Library
1400 Wilson Blvd.
Arlington, Virginia 22209
— 1 copy

Office of Naval Research
Physics Division Office (Code 412)
800 North Quincy Street
Arlington, Virginia 22217
— 2 copies

Office of Naval Research
Director, Technology (Code 200)
800 North Quincy Street
Arlington, Virginia 22217
— 1 copy

Naval Research Laboratory
Department of the Navy
Attn: Technical Library
Washington, DC 20375
— 1 copy

Office of the Director of Defense
Research and Engineering
Information Office Library Branch
The Pentagon
Washington, DC 20301
— 1 copy

U.S. Army Research Office
Box 1211
Research Triangle Park
North Carolina 27709
— 2 copies

Defense Technical Information Center
Cameron Station
Alexandria, Virginia 22314
— 12 copies

Director, National Bureau of Standards
Attn: Technical Library
Washington, DC 20234
— 1 copy

Director
U.S. Army Engineering Research
and Development Laboratories
Attn: Technical Documents Center
Fort Belvoir, Virginia 22060
— 1 copy

ODDR&E Advisory Group on Electron Devices
201 Varick Street
New York, New York 10014
— 1 copy

Air Force Office of Scientific Research
Department of the Air Force
Bolling AFB, DC 22209
— 1 copy

Air Force Weapons Laboratory
Technical Library
Kirtland Air Force Base
Albuquerque, New Mexico 87117
— 1 copy

Air Force Avionics Laboratory
Air Force Systems Command
Technical Library
Wright-Patterson Air Force Base
Dayton, Ohio 45433
— 1 copy

Lawrence Livermore Laboratory
Attn: Dr. W. F. Krupke
University of California
P.O. Box 808
Livermore, California 94550
— 1 copy

Harry Diamond Laboratories
Technical Library
2800 Powder Mill Road
Adelphi, Maryland 20783
— 1 copy

Naval Air Development Center
Attn: Technical Library
Johnsville
Warminster, Pennsylvania 18974
— 1 copy

Naval Weapons Center
Technical Library (Code 753)
China Lake, California 93555
— 1 copy

Naval Underwater Systems Center
Technical Center
New London, Connecticut 06320
— 1 copy

Commandant of the Marine Corps
Scientific Advisor (Code RD-1)
Washington, DC 20380
— 1 copy

Naval Ordnance Station
Technical Library
Indian Head, Maryland 20640
— 1 copy

Naval Postgraduate School
Technical Library (Code 0212)
Monterey, California 93940
— 1 copy

Naval Missile Center
Technical Library (Code 5632.2)
Point Mugu, California 93010
— 1 copy

Naval Ordnance Station
Technical Library
Louisville, Kentucky 40214
— 1 copy

Commanding Officer
Naval Ocean Research & Development Activity
Technical Library
NSTL Station, Mississippi 39529
— 1 copy

Naval Explosive Ordnance Disposal Facility
Technical Library
Indian Head, Maryland 20640
— 1 copy

Naval Ocean Systems Center
Technical Library
San Diego, California 92152
— 1 copy

Naval Surface Weapons Center
Technical Library
Silver Spring, Maryland 20910
— 1 copy

Naval Ship Research and Development Center
Central Library (Code L42 and L43)
Bethesda, Maryland 20084
— 1 copy

Naval Avionics Facility
Technical Library
Indianapolis, Indiana 46218
— 1 copy